Ana Pires de Almeida

Bachelor in Chemical and Biochemical Engineering

Formulation of ZSM-5 zeolite and UTSA-16 MOF by extrusion

Dissertation submitted in partial fulfillment
of the requirements for the degree of:

Master of Science in
Chemical and Biochemical Engineering

Adviser: Carlos Grande, Senior Research Scientist, SINTEF Industry

Co-advisers: Rui Ribeiro, Postdoctoral Researcher, NOVA University of Lisbon

José Paulo Barbosa Mota, Full Professor, NOVA University of Lisbon

FACULDADE DE CIÊNCIAS E TECNOLOGIA
UNIVERSIDADE NOVA DE LISBOA

March, 2018

Formulation of ZSM-5 zeolite and UTSA-16 MOF by extrusion

Faculdade de Ciências e Tecnologia, Universidade Nova de Lisboa.

Acknowledgments

This study was completed under an Erasmus Traineeship Programme at SINTEF, an independent research organisation in Norway.

Foremost, I would like to express my sincere gratitude to my advisor, Dr. Carlos Grande, who presented me with the opportunity to take part in this project, integrating me in the team at SINTEF in Oslo and allowing me to explore the available resources to improve my research. His guidance, suggestions and genuine concern helped steer this work in the right direction. I would like to express my great appreciation to my co-advisors: Dr. Rui Ribeiro, for the patient guidance, availability to answer my questions and very valuable reviews of this thesis; Prof. José Paulo Mota, without whom this exchange would not have been possible and for his enthusiastic encouragement.

I would like to extend my grateful thanks the members of staff at SINTEF for sharing their time and insight with me. I am particularly grateful to Ms Aud Spelkjavik, who tirelessly helped me with BET measurements, Ms Aud Bozuga, for her help in the adsorption measurements and Mr Paul McMahon for his guidance in compression testing. My special thanks are extended to the other students at SINTEF, who provided help on the lab, coffee break discussions and a support system away from home.

I am truly grateful to my loved ones, family and friends, who provided support and encouragement and without whom I would not have made it this far.

Finally, I wish to acknowledge the support provided by the Research Council of Norway through the CLIMIT program by the SINTERCAP project (233818). This publication has been produced with partial support from the BIGCCS Centre, performed under the Norwegian research program Centres for Environment-friendly Energy Research (FME). I wish to thank the following partners for their contributions: ConocoPhillips, Gassco, Shell, Statoil, TOTAL, GDF SUEZ and the Research Council of Norway (193816/S60).

Abstract

Porous materials are suitable for gas storage and separation applications. Synthesized as powders, these materials must be formulated to be handled in industrial settings. Formulation provides an optimized structure with improved mechanical and chemical stability. Extrusion is frequently employed and enables formulation using small amounts of solvent.

This work reports the formulation of zeolites and metal-organic frameworks (MOFs), namely ZSM-5 and UTSA-16. Pastes comprising the porous material, binders (colloidal silica and poly-vinyl alcohol, PVA) and plasticizers (water and propanol) are extruded into pellets in a four-step process comprising paste preparation, extrusion, drying and thermal treatment. The formulation process leads to slight surface area reduction in zeolite samples (9% decrease); more significant variation is observed in MOF extrudates (38% decrease). In both cases, lower binder content originates denser pellets. The density of ZSM-5 extrudates was similar to commercial zeolite pellets, while in UTSA-16 it was considerably superior.

The adsorption capacity of each formulated material for methane, carbon dioxide and water is measured. Both extrudates can adsorb methane and carbon dioxide. The amount of methane adsorbed is slightly higher on ZSM-5 extrudates, while UTSA-16 extrudates show higher selectivity than ZSM-5 for carbon dioxide molecules, adsorbing nearly twice as much. ZSM-5 extrudates show resistance to water, which is desirable for utilization in several industrial applications.

Keywords: Formulation; Extrusion; Zeolite; Metal-organic framework.

Resumo

Os materiais porosos podem ser aplicados em processos de separação e captura de gases. É necessário proceder à sua formulação para que estes materiais possam ser utilizados na indústria, uma vez que são sintetizados como pós. Esta técnica confere ao material uma estrutura optimizada, com aumento da sua estabilidade mecânica e química. A extrusão é o processo mais frequente e permite a formulação de materiais com recurso a quantidades reduzidas de solventes.

Este estudo descreve a formulação de zeólitos e redes metal-orgânico (MOF), nomeadamente ZSM-5 e UTSA-16. Pastas compostas por um material poroso, *binders* (silica colloidal e álcool poli-vinílico, PVA) e plastificantes (água e propanol) são extrudadas, formando pellets, num processo de quatro etapas: preparação da pasta, extrusão, secagem e tratamento térmico. O processo de formulação leva a uma ligeira diminuição de área superficial nas amostras de zeólito (redução de 9%); a variação observada nos extrudados de MOF é mais significativa (redução de 38%). Em ambos os casos, uma composição com menos *binders* origina pellets mais densas. A densidade dos extrudados de ZSM-5 obtidos é semelhante à de pellets de zeólito comerciais. No caso dos extrudados de UTSA-16, a densidade é consideravelmente superior.

A capacidade de adsorção de metano, dióxido de carbono e água foi avaliada para cada material formulado. Tanto os extrudados de zeólito como os de MOF adsorvem metano e dióxido de carbono. A quantidade de metano adsorvida nos extrudados de ZSM-5 é ligeiramente superior. O oposto ocorre no caso do dióxido de carbono: os extrudados de MOF adsorvem quase duas vezes mais do que os de zeólito. Extrudados de ZSM-5 mostram resistência à água, uma característica vantajosa para aplicação em diversas indústrias.

Palavras-chave: Formulação, Extrusão, Zeólito, Rede metal-orgânico.

Nomenclature

BET technique	Brunauer-Emmett-Teller technique
CH_4	Methane
CNG	Compressed Natural Gas
CO_2	Carbon dioxide
GWP	Global Warming Potential
IUPAC	International Union of Pure and Applied Chemistry
LNG	Liquid Natural Gas
MOF	Metal-Organic Framework
NGV	Natural Gas Vehicles
PCP	Porous Coordination Polymers, different denomination for MOFs
PVA	Polyvinyl Alcohol, $[CH_2CH(OH)]_n$
SEM	Scanning electron microscopy
UTSA-16	University of Texas San Antonio-16
	$\{[KCo_3(C_6H_4O_7)(C_6H_5O_7)(H_2O)_2]\cdot 8H_2O\}_n$
ZSM-5	Zeolite Socony Mobil-5, $[Na_nAl_nSi_{96-n}O_{192}\cdot 16H_2O]$, n<27
1-PrOH	1-Propanol, $CH_3CH_2CH_2OH$

Contents

1. Introduction 1
1.1 Context and motivation 1
1.2 Outline 3
2. Background 5
2.1 Adsorption 5
2.2 Adsorptives 8
2.3 Adsorbent Materials 9
2.3.1 Zeolites 10
2.3.2 Metal-Organic Frameworks 12
2.3.3 Formulation 14
3. Experimental Methods 17
3.1 Materials 17
3.2 Formulation 17
3.3 Characterization 22
3.4 Adsorption equilibrium measurements 24
4. Results and Discussion 27
4.1 Effect of additives 27
4.2 SEM Imaging 30
4.3 Mechanical strength 31
4.4 Surface area 33
4.5 Adsorption 35
5. Conclusions and Further Work 40
6. References 42

List of Figures

Figure 1 - Representation of the adsorption process of a gas on the surface of a porous solid [3], adapted. 5

Figure 2 – Types of physisorption isotherms, IUPAC classification [25]. Amount adsorbed plotted as function of the relative pressure p/p0, with p0 as saturation vapor pressure of the adsorptive… 6

Figure 3 - Evolution of verified Zeolite Framework Types, as reported by the Atlas of Zeolite Framework Types, 6th ed. (dark blue) and by the International Zeolite Association database, IZA-SC (light blue). 10

Figure 4 - ZSM-5 layer with pentasil chain outlined [37]. 11

Figure 5 - SEM image of powdered ZSM-5. 11

Figure 6 - Number of publications containing the keyword: "metal-organic framework". Source: Web of Science, 23 Jan 2018. 12

Figure 7 - SEM image of powdered UTSA-16. 13

Figure 8 - Stages of the formulation process by extrusion. 15

Figure 9 - Thermo Scientific Haake Minilab II extruder, at SINTEF Oslo. 17

Figure 10 – Internal part of the Thermo Scientific Haake Minilab II extruder available at SINTEF Oslo. 18

Figure 11 - Operating panel of the Thermo Scientific Haake Minilab II extruder available at SINTEF Oslo, during closed cycle extrusion, taken on 27/11/2017. 18

Figure 12 - ZSM-5 paste exiting the output channel, following extrusion. 19

Figure 13 - Preliminary step: UTSA-16 soaking in propanol. 21

Figure 14 - Extrusion paste. 21

Figure 15 - Extruder compartment following 5 minute, closed-cycle extrusion. 21

Figure 16 - Resulting UTSA-16 extrudate. 21

Figure 17 – Diagram of the compression test of a pellet, adapted from [77]. 23

Figure 18 – Graphic representation of binder composition in the ZSM-5 extrusion pastes. 27

Figure 19 - Effect of binder composition on ZSM-5 extrudates. 28

Figure 20 - Graphic representation of PVA and Propanol composition in the UTSA-16 extrusion pastes. 29

Figure 21 - UTSA-16 extrudates following extrusion and activation. 29

Figure 22 - ZSM-5 extrudate, sample 8.3. 30

Figure 23 - UTSA-16 extrudate, sample 9. 30

Figure 24 - ZSM-5 extrudate surface. 31

Figure 25 - UTSA-16 extrudate surface. 31

Figure 26 - Powdered ZSM-5. 31

Figure 27 - Powdered UTSA-16. 31

Figure 28 - Compression test results, two pellets of the same ZSM-5 extrudate sample. (Commercial 4A zeolite extrudate reported result for comparison [71]) 32

Figure 29 - Compression test results, two pellets of the same UTSA-16 extrudate sample. (Commercial 4A zeolite extrudate reported result for comparison [71]). 32

Figure 30 – Force applied on ZSM-5 extrudates in relation to Silica content. 32

Figure 31 – Force applied on UTSA-16 extrudates in relation to PVA content. 32

Figure 32 – Force applied on ZSM-5 extrudates in relation to sample density. 33

Figure 33 - Force applied on UTSA-16 extrudates in relation to binder content. 33

Figure 34 - N2 adsorption isotherms at 77 K for ZSM-5 powder and extrudate. 33

Figure 35 – N_2 adsorption isotherms at 77 K for UTSA-16 extrudates and powder. 33

Figure 36 - Surface area decrease in relation to the pristine powder as function of the binder content, activation at 773K. 34

Figure 37 – Surface area decrease in relation to the pristine powder as function of the binder content, activation at 393K. 34

Figure 38 - Adsorption equilibrium of CH_4 on ZSM-5 extrudates at 303, 323, and 343 K. The filled symbols denote adsorption data and open symbols denote desorption data. Solid lines are fittings from the Langmuir isotherm. 35

Figure 39 - Adsorption equilibrium of CO_2 on ZSM-5 extrudates at 303, 323, and 343 K. The filled symbols denote adsorption data and open symbols denote desorption data. Solid lines are fittings from the Langmuir isotherm. 35

Figure 40 – Isosteric heat as a function of loading. Dashed lines represent the ΔH parameter employed in the Langmuir fitting. 36

Figure 41 – CO_2/CH_4 selectivity as a function of pressure. 36

Figure 42 – Adsorption equilibrium of H_2O on ZSM-5 extrudates at 303, 323, and 343 K, not modelled. 36

Figure 43 – Adsorption equilibrium of CH_4 on UTSA-16 extrudates at 303, 323, and 343 K. The filled symbols denote adsorption data and open symbols denote desorption data. Solid lines are fittings from the Langmuir isotherm. 37

Figure 44 – Adsorption equilibrium of CO_2, on UTSA-16 extrudates at 303, 323, and 343 K. The filled symbols denote adsorption data and open symbols denote desorption data. Solid lines are fittings from the Langmuir isotherm.. 37

Figure 45 - Isosteric heat as a function of loading. Dashed lines represent the ΔH parameter employed in the Langmuir fitting. 38

Figure 46 - CO_2/CH_4 selectivity as a function of pressure. 38

Figure 47 - Adsorption equilibrium of H_2O on UTSA-16 extrudates at 303, 323, and 343 K, not modelled. 38

List of Tables

Table 1 - IUPAC pore classification according to their size. 9

Table 2 - Characteristics of ZSM-5 zeolite powder. 11

Table 3 - Characteristics of UTSA-16 MOF powder. 13

Table 4 - Composition of ZSM-5 extrusion pastes, amounts in grams. 20

Table 5 - Relation between composition and extrudate density in ZSM-5 extrudates. 29

Table 6 - Relation between composition and extrudate density in UTSA-16 extrudates. 30

Table 7 - Textural results for best formulation compositions. 34

Table 8 - Langmuir parameters of CH4 and CO2 adsorption on ZSM-5 and UTSA-16 extrudates. 39

1. Introduction

1.1 Context and motivation

Energy is the foundation of all living systems and throughout time mankind acknowledged its potential. In fact, capture, collection and utilization of energy are pivotal to economic and social transformation and development. Population global growth and fast emergence of developing economies are driving a huge increase in energy demand.

Fossil fuels provide over 85% of all energy used, remaining the leading source of energy worldwide because of their high calorific value and reasonable cost [1]. Recently, the depletion of fossil fuel resources and the impact of the greenhouse gases generated by their combustion (e.g. carbon dioxide, CO_2, and methane, CH_4) has increased awareness of environmental issues.

Natural gas is originated from the decomposition of organic matter and trapped beneath the surface of the Earth in terrestrial or oceanic deposits. It is mainly composed of methane (55% to 98% in volume) which retains a high Global Warming Potential (GWP), making it essential to prevent accidental release into the atmosphere in every stage of application [2].

Natural gas currently supplies around 25% of all energy produced and its use is expected to increase in the future. The combustion of this fuel yields mostly water vapour and CO_2 emissions in significantly lower amounts per unit of produced energy than those generated by oil or charcoal combustion [2]. This makes natural gas the cleanest of fossil fuels, regarded as an alternative to petroleum in the automobile industry.

Engineering developments in drilling techniques revealed larger gas reserves than previously known. Still, some drawbacks hinder a widespread use of this fuel: under atmospheric conditions, natural gas is a gaseous fluid with lower volumetric energy density than liquid fuels. Storage by compression (compressed natural gas, CNG) or liquefaction (liquified natural gas, LNG) can decrease this gap but require high pressure, overly expensive technology [3], [4].

Biogas is formed through the anaerobic decomposition of organic matter and is primarily composed of methane and carbon dioxide. Other components include oxygen, and nitrogen from air, water and sulphur compounds. It can be used to produce electricity, heat, fuel vehicles and for injection in natural gas grids. Separation of

components to upgrade biogas into biomethane is made sequentially, starting with removal of hazardous sulphur compounds and water, followed by the separation of the CH_4 and CO_2 mixture [5], [6].

Mitigation of climate change caused by greenhouse gas accumulation in the atmosphere represents a major and urgent challenge for the 21st century. As advances in the establishment of zero-carbon sources at significant levels will entail decades of R&D [7], continued dependence on fossil fuels is expectable. Extensive reduction of greenhouse gas emissions is thus vital to prevent a further rise of global temperature.

The industrial application of gases for energy production involves complex separation and purification processes. These are used for removal of impurities from gaseous mixtures, bulk separations and gas storage [8]. Gas adsorption techniques have been increasingly implemented for this purpose because of their flexible design nature and high efficiency. The storage of natural gas has been a target of research for nearly 50 years [9] and may be applied to natural gas vehicles (NGVs), mobile tankers and cylinders or large-scale storage on distribution pipelines [10]. The capture and storage of CO_2 using adsorption techniques is also under extensive study as an essential strategy for reduction of atmospheric greenhouse gas concentration [11].

Solid microporous materials with large sorptive capacities can store considerable amounts of gases at relatively low pressures. Early research was focused on activated carbons and zeolite adsorbents; the extensive study of new structures and applications for these materials has led to the targeted design and synthesis of porous solids with high selectivity for specific applications [12]. Metal-organic frameworks (MOFs) are a new generation of adsorbents that has received a lot of attention for their outstanding features for gas storage and separation [13]. Tuneable pore surface paired with extremely high porosity are responsible for considerable improvements in the performance of these new materials.

Porous materials are synthesised in powdered form. Shaping strategies are essential for large-scale application as they ensure the optimization of packing within large reactors or tanks while maintaining the powdered material's properties, improving performance and reducing process cost [14]. Several techniques are under study for formulation of porous materials. The most widely used method, extrusion, allows for formulation using little or no solvent. The reduction of solvent use is a critical aspect for implementation of more sustainable chemical processes with industrial application. However, the main challenge to industrial implementation of this method is scalability [15]. Considering its relevance, this aspect is relatively under-examined, with only a small number of articles on formulation being published yearly.

The objective of this study is the formulation of powdered zeolites and MOFs into pellets using extrusion techniques. For this purpose, each extrusion paste is prepared using the porous material (ZSM-5 or UTSA-16), binders (PVA and silica) and plasticizers (water and propanol). Characterization techniques are applied for the

evaluation of material properties following extrusion. The adsorption capacity of each material for methane, carbon dioxide and water are measured.

1.2 Outline

This study will address the formulation of zeolites and metal-organic frameworks by extrusion. The formulated extrudates will be characterized by basic techniques and evaluated for gas adsorption purposes.

The study is structured as follows:

Chapter 2: Background
Explanation of major theoretical concepts, general definitions and terminology concerning adsorption at the gas/solid interface and porous materials.

Chapter 3: Materials and experimental methods
Description of all experimental work, from formulation of the adsorbent materials to their characterization and adsorption evaluation, including method references and experimental methodology employed.

Chapter 4: Results and Discussion
Description, explanation and interpretation of the experimental results and key findings, in particular the effect of paste composition and processing on the characteristics of extrudates and their adsorptive capacity.

Chapter 5: Conclusions and future work
Summary of findings and analysis of significance of the study. Highlight on opportunities for future research.

A table of nomenclature including acronyms used throughout the text is provided before the index.

2. Background

2.1 Adsorption

Frequent and naturally occurring, sorption processes have long been known. These mechanisms involve the removal of a substance (sorptive) from the surrounding medium by a mass separating agent (sorbent). One of these phenomena, adsorption, is defined as the enrichment of fluid density at an interfacial layer. Removal occurs by spontaneous adhesion of a gas or liquid adsorptive to the surface of the adsorbent. Attraction forces between adsorbent and adsorptive cause the release of energy, thus the process is exothermic [16].

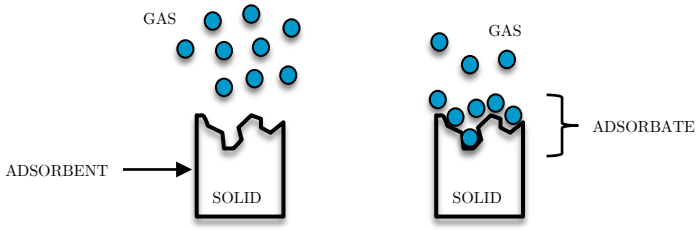

Figure 1 - Representation of the adsorption process of a gas on the surface of a porous solid [3], adapted.

In cyclic adsorption processes, the term desorption or regeneration describes the process approached from the opposite equilibrium direction. In this stage, the bonds within the adsorbate complex are broken, and adsorbate molecules removed from the surface of the adsorbent. The capacity of the adsorbent is regenerated, and valuable elements can be recovered. Desorption does not occur spontaneously; it may be induced by pressure reduction, temperature increase or addition of a competitive adsorptive [17], [18].

Useful products can be obtained from both steps: the effluent during the adsorption stage corresponds to the purified "raffinate" product and the strongly adsorbed species recovered in concentrate form during the regeneration step are called the "extract" products [19].

The separation by adsorption follows one of three mechanisms: steric, kinetic and equilibrium mechanisms. In the steric mechanism, the dimension of pores within a porous material allows small molecules with the right shape to be diffused into them, keeping out any other molecules. Kinetic separation is based on the different diffusing rates of different adsorptives, meaning the time of exposure dictates which species is preferentially removed. The equilibrium mechanism relies on the adsorbent's ability to accommodate different species, causing the stronger adsorbing species to be preferentially removed from the fluid phase [20], [21].

The type of bond formed between adsorptive molecules and the adsorbent surface enables a distinction between two types of adsorption: physical (physisorption) and

chemical (chemisorption). Physisorption processes are characterized by weak interaction forces between molecules, based on Van der Waals forces or electrostatic interactions. They present a relatively low heat of adsorption and reversible character, meaning the adsorbent can be regenerated. Most gas adsorption processes comprise this kind of interactions [17], [18], [22], [23]. Chemisorption processes entail chemical interactions within the adsorbate-adsorbent system. The formation of ionic or covalent bonds requires intense heat of adsorption and is highly specific. Often irreversible, chemisorption may involve dissociation of the adsorbed species [18], [22].

Classification of adsorption isotherms

Adsorption equilibrium is commonly reported in the form of isotherms, which can be described as a relation between the quantity adsorbed and a given equilibrium pressure, or concentration of gas, at constant temperature. When the adsorption and desorption branches of the isotherm are not coincident, adsorption hysteresis arises [21].

Different gas physisorption systems present characteristic isotherm curves, most of them fitting into one of the six types shown in Figure 2. This classification depends on the strength of surface interactions and porosity of the material. The shape of these curves can provide relevant information on the pore structure of the adsorbent [24]–[26].

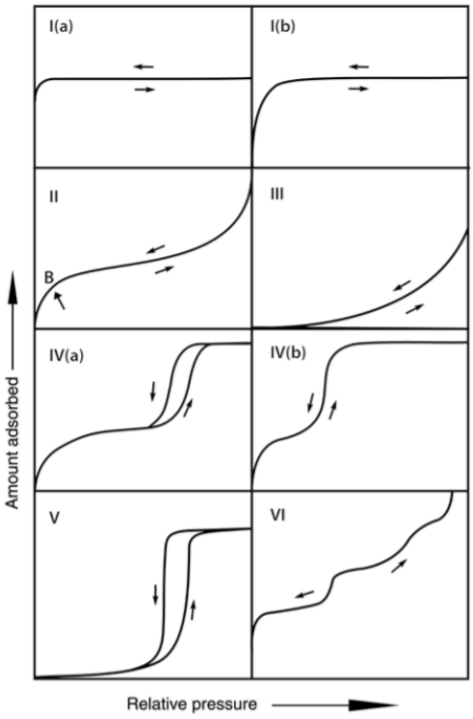

Figure 2 – Types of physisorption isotherms, IUPAC classification [25]. Amount adsorbed plotted as function of the relative pressure p/p0, with p0 as saturation vapor pressure of the adsorptive.

Type I are reversible adsorption isotherms that rise sharply at low pressures, reaching a plateau as relative pressure approaches 1. These are common in microporous solids, when the gas uptake is limited by micropore volume. Smaller pore widths cause higher adsorption energy and lower the micropore-filling pressure. Type I(a) isotherms are given by microporous materials having mainly narrow micropores while type I(b) isotherms are delivered by materials with pore size distributions over a wider range including wide micropores and narrow mesopores [24]–[27].

Type II reversible isotherms progress from concave to the p/p^0 axis to almost linear and then convex to the p/p^0 axis. These are obtained with solids that enable unrestricted multimolecular adsorption at high relative pressures, such as microporous or non-porous adsorbents. Point B indicates complete monolayer coverage and the outset of the multilayer adsorption stage [24], [27], [26].

Type III isotherms are convex to the p/p^0 axis. These uncommon, reversible isotherms are indicative of weak adsorbate interactions within a microporous or non-porous adsorbent [18–20].

Type IV isotherms are completely reversible and present a similar shape to *type II* isotherms at an early stage, reaching a saturation plateau at high relative pressures. These are obtained with mesoporous adsorbents and present a characteristic hysteresis loop, resultant from capillarity condensation within the pores. Type IV(a) isotherm hysteresis is due to capillary condensation. Adsorbents having smaller width mesopores present completely reversible Type IV(b) isotherms. These are also given by conical and cylindrical mesopores with closed tapered end [24]–[27].

Type V isotherms are related to *type III* isotherms, initially convex to the p/p^0 axis but reaching a plateau at high relative pressures. They are quite uncommon and present a hysteresis loop, related to the process of filling and emptying pores [24], [27], [26].

Type VI isotherms occur in subsequent steps dependant on the system and temperature. These uncommon isotherms are related to layer-by-layer adsorption on very uniform surfaces [24], [27], [26].

This classification system applies only to single component adsorption. Many isotherms have a more complex nature, not fitting into this classification list.

2.2 Adsorptives

In an adsorption process, the adsorptives correspond to the fluid phase that adheres to the surface of an adsorbent. In this work, methane, carbon dioxide and water are employed in adsorption equilibria studies.

Methane

Methane (CH_4) is an odourless but flammable gas, generally stable but explosive when mixed with air containing 5% to 14% of methane. Produced by anaerobic bacterial decomposition of matter in the presence of water, methane can be used in hydrogen production, manufacture of ammoniac and fertilizers, among others [3].

Naturally produced methane is mostly offset by natural mechanisms, however great amounts are produced by anthropogenic activity causing increasing concentration of this gas in the atmosphere. The growth in use of natural gas results in direct release of methane that represents a considerable environmental issue because methane is around 21 times more potent than CO2 as greenhouse gas, trapping larger amounts of heat at the surface of the planet [2].

It is considered a potential transition fuel for the automobile sector because it is naturally abundant and results in lower CO_2 emission than petroleum [28].

Carbon Dioxide

Carbon dioxide (CO_2) is an odourless, nontoxic and non-flammable gas. It presents linear geometry and nonpolar character, comprising two oxygen atoms double covalently bonded to a single carbon at an angle of 180^{o}.

This stable molecule is produced in large amounts by combustion of fossil fuels for the industrial and automotive sectors [28]. Industrialization, through the extensive use of non-renewable sources of energy, is responsible for a sharp increase in concentration of CO_2 in the atmosphere. Being a greenhouse gas, this variation led to the increase of global temperatures. For this reason, technologies and materials for capture and storage of CO_2 have been studied extensively as an urgent response for mitigation of the environmental impact of carbon-based fuels [7].

Water

Colourless and odourless, water (H_2O) is a polar molecule, commonly used as solvent. When used for adsorption, it provides information about surface interactions, adsorbent stability and moisture resistance, essential for application in an industrial setting [29].

2.3 Adsorbent Materials

Being a surface phenomenon, adsorption depends directly on the properties of the adsorbent. The surface area, pore network dimension and chemical properties of the adsorbent are crucial aspects in achieving a high adsorptive capacity that enables the material to interact with atoms and molecules at the surface but also throughout their bulk region [21].

Small particles exhibit high external surface areas, making fine particle powders great adsorbents. However, surface area in porous materials mostly depends on the amount and dimension of pores. A solid presenting a combination of micropore and macropore range pores provides optimal surface areas [21].

Porosity can be described as a ratio between pore volume and solid volume. The IUPAC recommendation for pore size classification is presented in Table 1 [27]. This is an arbitrary classification, based on nitrogen adsorption on a range of porous solids at boiling temperature [21].

Table 1 - IUPAC pore classification according to their size.

Classification	Pore width (nm)
Micropores	< 2
Mesopores	$2 < d < 50$
Macropores	> 50

Within a porous solid, gas molecules become surrounded by pore walls, which increase the interaction forces between them. In smaller pores, the interaction potentials of each wall overlap, greatly enhancing adsorption performance [24].

Several materials may be used as adsorbents. Activated carbon, zeolites, silica gel and activated alumina are the most widely used for commercial purposes, having large application in chemical, petrochemical and pharmaceutical industries.

In the past decades, enormous advances have been made in tailored design and synthesis of porous materials [30]. The formulation of superior sorbents can greatly impact the productivity of industrial processes. Future progress in the adsorption field depends on the development of new sorbents with improved characteristics, tailored to specific applications [12].

Currently, the development of innovative sorbent materials is strongly focused on clean, sustainable processes. The design of sorbents has moved from an empirical process to become the product of careful theoretical study, followed by molecular simulation.

2.3.1 Zeolites

Known for hundreds of years, natural zeolites have been object of study since the 18th century. Research on adsorptive properties for air purification and separation was initiated in the late 1940s and the first successful synthesis of zeolites was reported one decade later [31]–[33]. With high surface areas and crushing strength, these materials showed great potential for application as catalysts and adsorbents. Because of their interesting properties, several studies on synthesis and properties of zeolites have been published, resulting in a rapid development of synthetic zeolite framework types over the last decades, as illustrated in Figure 3 [34].

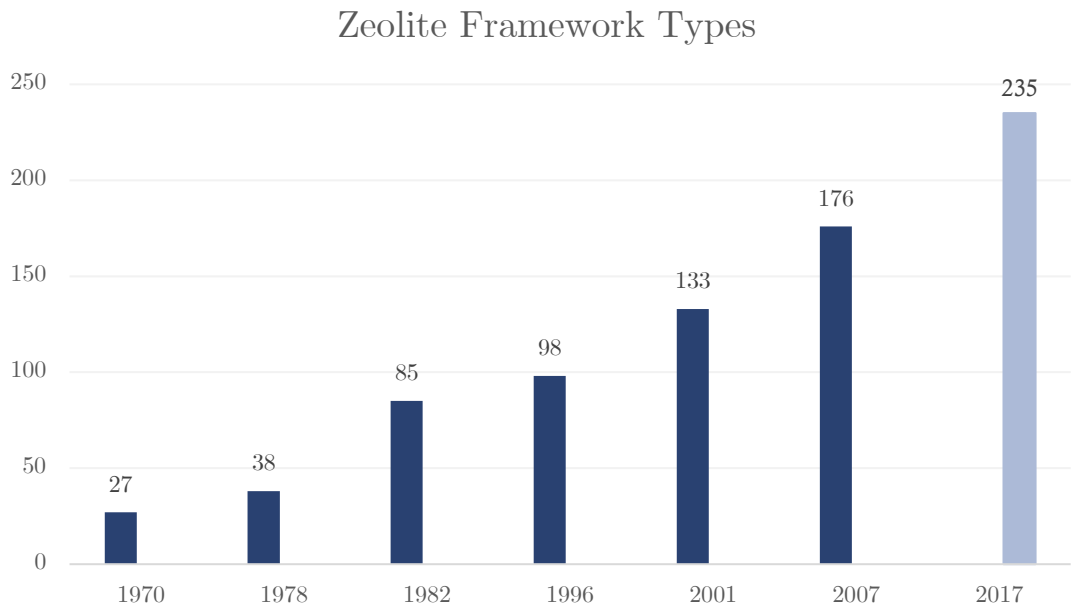

Figure 3 - Evolution of verified Zeolite Framework Types, as reported by the Atlas of Zeolite Framework Types, 6th ed. (dark blue) and by the International Zeolite Association database, IZA-SC (light blue).

Zeolites are a broad class of microporous, crystalline aluminosilicate materials. Composed of three-dimensional tetrahedral frameworks with densities of 19 to 21 T-atoms (Si, Al, P, Ga, Ge, B, Be, etc.) per 1000 Å^3 [34], these sorbents present cavities in uniform size, shape and structure. Rings composed of T- and O-atoms form intra-crystalline channels of pores, measuring 0.2 to 0.8 nm and with volumes of 0.10 to 0.35 cm^3/g.

Zeolites are typically very stable to temperature variations, which have been shown to confer flexibility to the framework [35]. Synthesis conditions determine the framework composition. Through post synthesis modifications, it is possible to vary the Si/Al ratio, affecting the hydrothermal stability and hydrophobicity of the material [36].

In addition to remarkable properties, low cost has contributed for the broad use of zeolites as catalysts and adsorbents.

ZSM-5

The ZSM-5 (Zeolite Socony Mobil-5), is a MFI framework type patented by Mobil in 1975 [34]. Traditionally used in the fields of petrochemistry and oil refining, this aluminosilicate pentasil zeolite has a high silica content and approximately cylindrical pores. It presents a linked tetrahedral configuration consisting of chains of eight 5-membered rings, the pentasil units, bonded by oxygen bridges. The pore size of the straight 10-member ring channels, y axis orientation, is estimated to be 5.4-5.6 Å, while that of the sinusoidal channels, x axis orientation, is of 5.1 – 5.4 Å [37].

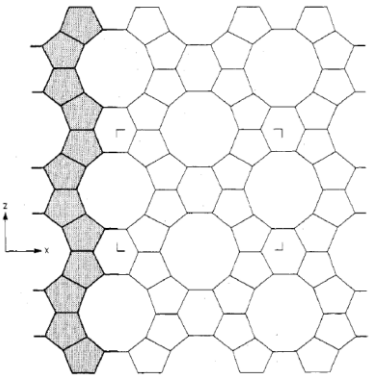

Figure 4 - ZSM-5 layer with pentasil chain outlined [37].

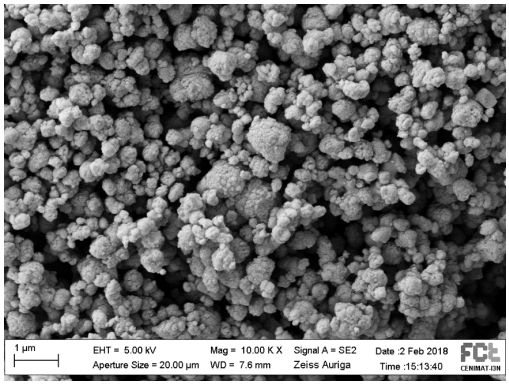

Figure 5 - SEM image of powdered ZSM-5.

The channel structure, specific pore size and shape and high thermal stability of this material render it desirable for gas separation applications. ZSM-5 has been successfully adopted as methane and carbon dioxide adsorbent [38].

Table 2 - Characteristics of ZSM-5 zeolite powder.

H-ZSM5 zeolite powder	
Chemical formula	$[H_nAl_nSi_{96-n}O_{192}\cdot 16H_2O]$, n<27
SiO_2/Al_2O_3 ratio	200
BET Surface area	341 m^2g^{-1}

2.3.2 Metal-Organic Frameworks

Metal-Organic Frameworks (MOFs), also known as porous coordination polymers (PCPs), are an emerging class of highly crystalline porous materials. Composed of networks of organic ligands (*linkers*) and metals (*secondary building unit*, *SBU*) and connected by strong coordination bonds, these materials form complex, porous frameworks. MOFs display extremely high porosity (up to 90%) and surface areas reaching above 10 000 m^2/g, the highest known for any porous material [39]–[41]. Due to their remarkable properties, this class of materials presents outstanding adsorption capacity, applied in gas storage [42], catalysis [43], [44], gas separation [13], electronic [45], [46] and medical applications [47].

Although the first reports on coordination compounds date from the late 1950s and early 1960s [48]–[50], it was not until the turn of the century that this class of materials started to get more attention from the scientific community and the potential of MOFs was noticed [51]–[54]. The remarkable features of these materials quickly generated great interest, leading to an incredibly fast development of this field. Nowadays, with ca. 70,000 different MOF structures on report at the Cambridge Crystallographic Data Centre [55] and thousands of papers published, MOFs have become ubiquitous and their study continues developing at a fast pace.

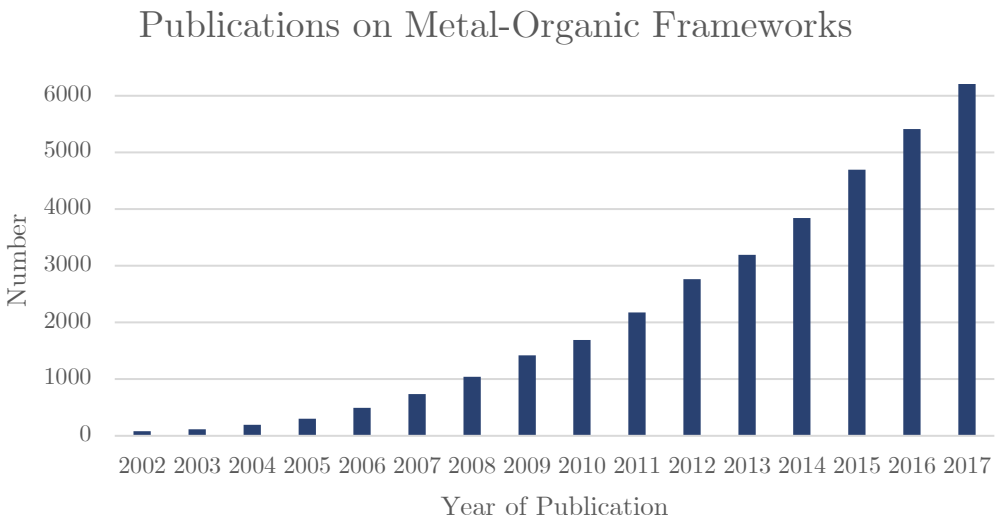

Figure 6 - Number of publications containing the keyword: "metal-organic framework". Source: Web of Science, 23 Jan 2018.

During the past two decades of research, the focus was in the development of structures and investigation on their applications [56], [57]. The modular nature of MOFs enables countless combinations of the organic and inorganic structural blocks that shape these frameworks. This choice influences framework topology and functionality although the determination of ideal synthesis conditions for a specific structure involves substantial trial and error. As an alternative process, computational simulations enable the rapid study of hypothetical structures for property prediction and structure identification. In

spite of being at an early stage, this process greatly increases the feasibility of precise tailoring and optimization of structural properties [58].

An interesting feature that has arisen from the extensive development of new MOFs is framework flexibility. Structures present dynamic behaviour, exhibiting larger ability to withstand physical or chemical transformations [59]. Understanding the link between framework geometry, chemical composition and the material's response to stimuli should enable the creation of materials with specific responses and the development of guidelines for the synthesis of novel materials [12].

UTSA-16

The UTSA-16 (University of Texas San Antonio-16) is a cobalt acetate – citric acid - based MOF. Its 3-D structure is shaped by tetrahedral Co(II) atoms and tetranuclear cobalt citrate clusters bonded in octahedral geometry.

This highly porous framework shape can be compared to an infinite anatase crystal structure, showing open interconnected channels of large dimensions (9.5 x 4.3 Å) along the x and y axis orientation [60], [61].

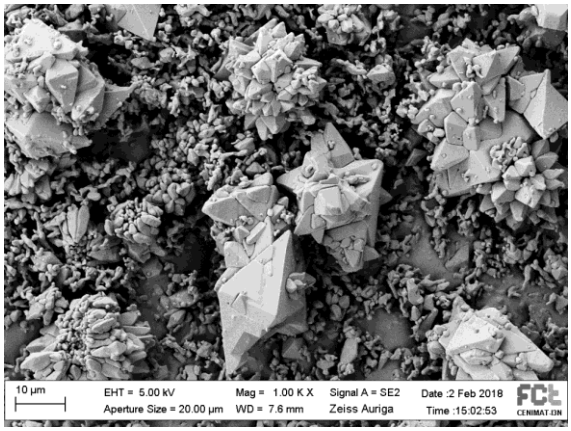

Figure 7 - SEM image of powdered UTSA-16.

The structure of this antiferromagnetic MOF has shown great potential for CO_2 capture applications [55, 56]. A hydrogen purification cycle from steam-methane reforming off-gas has been reported, offering high recovery and productivity yields [63].

Table 3 - Characteristics of UTSA-16 MOF powder.

UTSA-16 MOF powder	
Chemical formula	$\{[KCo_3(C_6H_4O_7)(C_6H_5O_7)(H_2O)_2]\cdot 8H_2O\}_n$
BET Surface area	837.05 m^2g^{-1}
Total pore volume	0.315 cm^3g^{-1}

2.3.3 Formulation

Adsorbents are usually synthesized as small crystals in powdered form. To be suited for industrial application, these hierarchically microporous materials must be formulated into macroscopic shapes such as spheres, pellets or monoliths. Their use as high performance adsorbents in cyclic adsorption processes depends on the chemical and mechanical properties of the structured material. For that reason, formulation is an essential step that should provide an optimized structure for efficient gas flow and mass transfer without property deterioration [64].

The shaping process and the selected shape of the adsorbent affect important parameters, such as the external surface area, pressure drop (through the adsorbent bed), adsorbent loading (amount of adsorbent in given volume), void volume and channelling and dispersion characteristics [64]. These geometric parameters greatly impact the size of the equipment, product recovery, power consumption and, consequently, the overall performance and cost of the process [14].

The formulation process involves the selection, mixing and shaping of component materials (active phase + additives). The primary function of each additive and the behaviour of the complex mixture must be taken into consideration [65]. Common processing techniques for adsorbent formulation include extrusion, coating, colloidal processing and templating. The shaping process is followed by a thermal treatment to retain shape [66].

Despite the growing interest in porous materials and their potential application in industrial processes, few articles addressing structuring and formulation processes have been published. Current research is focused on the efficient shaping of materials with preservation or improvement of properties, easing handling and storage [67], [68].

Extrusion

Extrusion processes involve the movement of a material through a confined space using little to no solvents. Most often, the movement is propelled by a set of screws that pushes the material forward. This technique may involve the use of one single screw, Single Screw Extrusion (SSE) or twin screws, Twin Screw Extrusion (TSE). In the extrusion process, materials are mixed, heated and shaped while strong compression and shear forces are exerted [15].

Described for the first time by Joseph Bramah in 1797, in a patent for a lead pipe manufacturing process, extrusion processes are nowadays well established and commonly applied in industrial processes (manufacture of metals, polymers, pharmaceuticals, food). More recently found to efficiently process porous materials in a solvent-free environment, extrusion is the most frequently employed technique applied in structuring and formulating powders for adsorption and catalysis [69], [70].

Often, the porous material does not naturally possess the necessary plasticity to undergo extrusion; the high levels of compression and shearing it is exposed to may lead to destruction of the porous structure, rendering the material amorphous. To prevent it, the porous media is mixed with additional substances forming a paste with improved rheological properties [69]. The extrusion paste is composed of the powdered porous material, a binder that provides mechanical strength and mouldability, and a plasticizer that serves as wetting agent and decreases the viscosity of the mixture, forming a plastic composition. Optionally, a dispersant can be added to avoid agglomeration [66], [70], [71].

Several types of binder exist: Clays [72], alumina [73] and silica [74] are commonly used and should provide hardness to the extrudates. Organic additives may also be added, increasing the strength of the extrudate and reducing shape variations. Cellulose [75], methylcellulose [76] and polyvinyl alcohol (PVA) [74] are the most common additives. The selection of appropriate binders and their proportions is complex and depends on the composition of the adsorbent, as well as desired shape.

Water is the most used plasticizer, though organic solvent-water mixes are also common [71]. Plasticizers can usually be removed by heating (or vacuum) after extrusion by controlled burning, resulting in macro-porosity. Certain porous materials, such as MOFs, cannot withstand such high temperatures without severe structural damage. Therefore, alternative approaches are needed when using this kind of porous solids.

The stages of the extrudate formulation process are usually the paste preparation, followed by extrusion, drying, and thermal treatment, as illustrated in Figure 8.

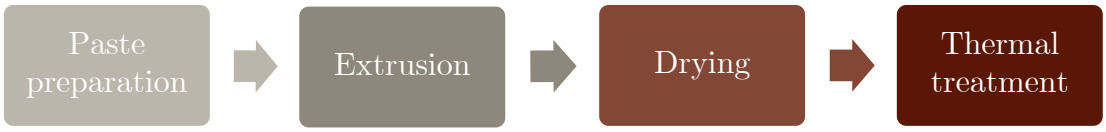

Figure 8 - Stages of the formulation process by extrusion.

The paste preparation step is frequently divided into a dry mixing step, followed by addition of liquid plasticizers and subsequent kneading until homogeneity of the paste is achieved. During the extrusion step the paste is extruded through a die of adjustable size and shape. The drying stage is planned so the sample will dry evenly without changing shape or forming cracks. Finally, the thermal treatment ensures the removal of binders and plasticizers, maintaining the high surface area of the porous material.

The development of sustainable industrial processes using porous adsorbents depends on the scalability of this technique, reducing the effects of pore blocking and crystal structure damage .

3. Experimental Methods

3.1 Materials

Adsorbents: ZSM-5 (Clariant), UTSA-16 (Obtained by hydrothermal synthesis, as described in the literature [62], [63]).

Binders: Polyvinyl alcohol (PVA, Aldrich) and colloidal silica (LUDOX® LS, 220m^2/g, 30 wt%, Aldrich).

Plasticizers: water and propanol (1-Propanol, Sigma-Aldrich)

3.2 Formulation

The first step in the formulation process is the preparation of an extrusion paste. It should improve the rheological properties of the powdered adsorbent, letting it undergo extrusion without or with minimal damage to its physical properties.

One of the challenges in paste preparation is the identification of binders and plasticizers that yield favourable mechanical properties, maintaining adequate surface area. Different sets of binders and plasticizers are used for the ZSM-5 and the UTSA-16 pastes, in accordance with the characteristics of each material.

Extrusion was selected as processing method and all pastes formulated into pellets with 2 mm diameter. The equipment used for extrusion, Thermo Scientific HAAKE MiniLab II – Micro Rheology Compounder, is a twin-screw extruder (TSE) equipped with two co- or counter-rotating screws that transport the material along a barrel, exposing it to high compression forces and shearing. It compounds 5 g or 7 cm^3 samples (amount strongly related to sample density).

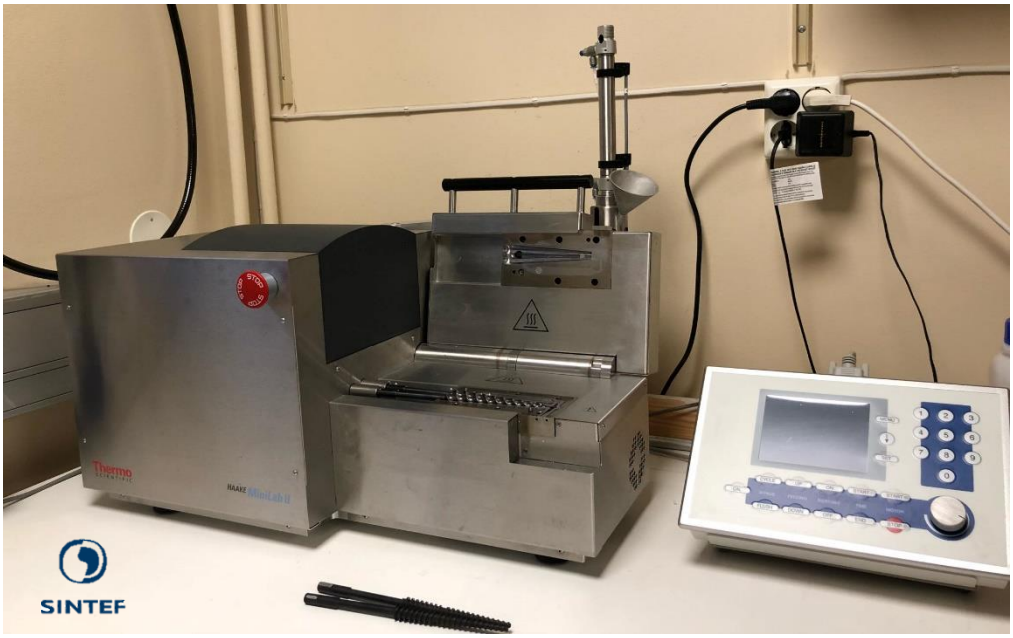

Figure 9 - Thermo Scientific Haake Minilab II extruder, at SINTEF Oslo.

This extruder is equipped with a backflow channel and an automatic bypass valve that allow the operator to work with well-defined residence times. The backflow channel includes two pressure transducers (p1 and p2, Figure 10) that enable the measurement of the relative melt viscosity.

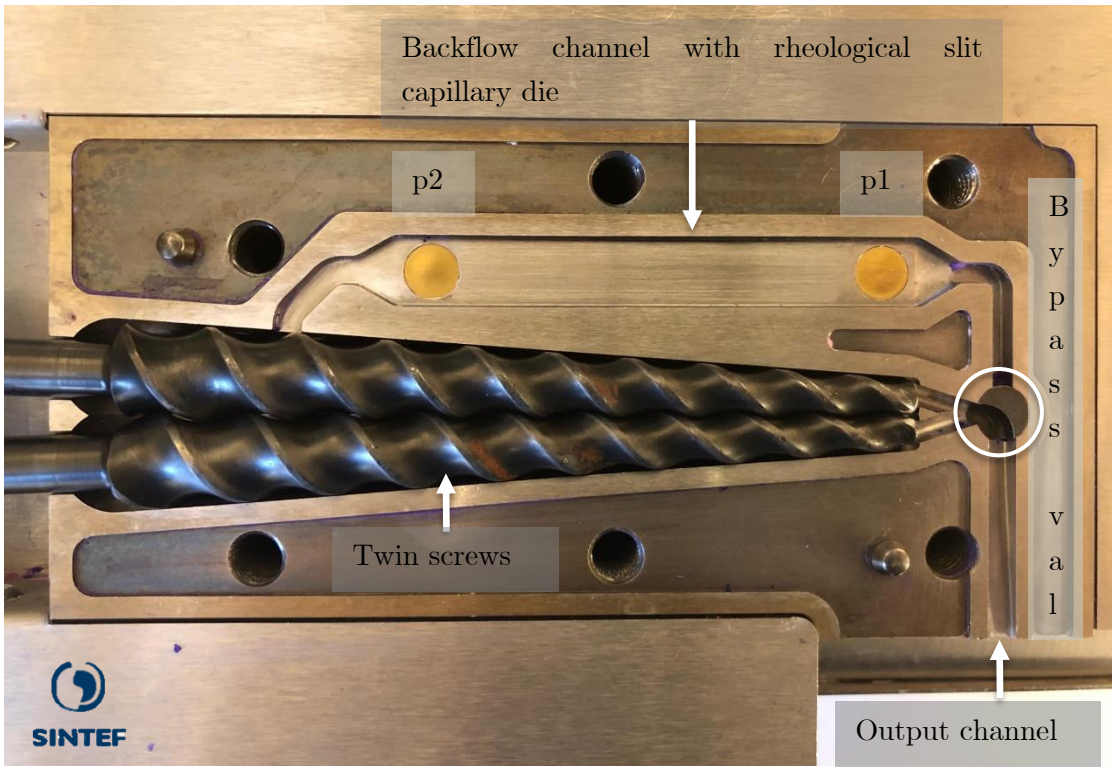

Figure 10 – Internal part of the Thermo Scientific Haake Minilab II extruder available at SINTEF Oslo.

The operating panel is composed of an LCD screen. Temperature, torque, rotation frequency, measurement time and volume stream can be set before each measurement. While measurement is in progress, instant readings of time, temperature, pressure, torque and speed are displayed. When the test is completed, the material is extruded as a strand, through a 2mm die.

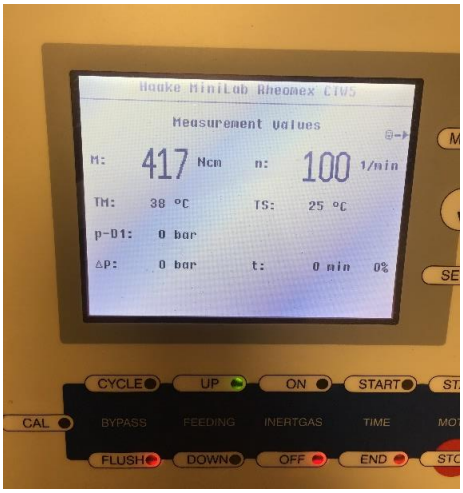

Figure 11 - Operating panel of the Thermo Scientific Haake Minilab II extruder available at SINTEF Oslo, during closed cycle extrusion, taken on 27/11/2017.

During the drying stage, the extrudates lose water and propanol by evaporation from the surface, which may cause the sample to shrink, crack or alter its shape. Following extrusion, the samples are allowed to air dry at constant temperature (298 K) for at least 24h. This step should allow the samples to solidify and later go through thermal treatment without suffering great shape variation.

The thermal treatment or "firing" stage consists of gradually heating samples to temperatures above 700 K. This process enables the removal of plasticizers and temporary binders, generating macroporosity within the extruded sample. The zeolite samples undergo thermal treatment at 773 K for 12h. MOFs do not have such a high thermal stability, meaning they cannot withstand the firing stage without damaging the crystalline structure. UTSA-16 extrudate activation is performed at temperatures up to 393 K, in accordance with limits established in previous research [71].

ZSM-5 extrudates:

Commercial ZSM-5 extrudates (prepared and distributed by Clariant) are prepared using alumina as binder. It should be noted that, in this study, the ZSM-5 extrusion paste is prepared using a mixture of powdered ZSM-5 zeolite, PVA as temporary binder, colloidal silica as permanent binder and water as plasticizer. The added silica content should increase the material's selectivity to methane.

ZSM-5 powder is weighed; PVA added and (dry) mixed. Water and Ludox added in appropriate amounts. The paste is thoroughly blended for 5 - 10 min and put through the extruder in open or closed cycle for 5 minutes. The extrudate is collected and allowed to air-dry for 24 hours. Calcination is performed at 773 K.

Several compositions were prepared and tested. Variations were imposed on the ratio of zeolite/binders and their effect on the properties of the material was analysed. The composition of the extrudates is detailed on Table 4, including only the trials that retained shape successfully and were selected for further characterization.

Note that PVA presents low solubility in water. To prevent a variable binder content throughout the paste, the PVA should have been diluted in water and integrated in the paste as a solution.

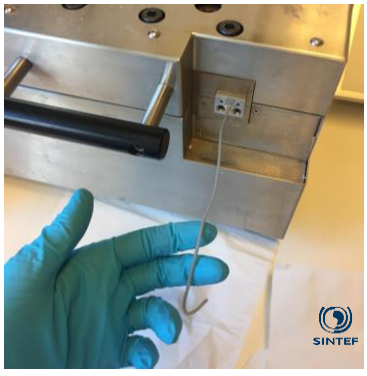

Figure 12 - ZSM-5 paste exiting the output channel, following extrusion.

Table 4 - Composition of ZSM-5 extrusion pastes, amounts in grams.

	Trial 4		Trial 5		Trial 6		Trial 7.2	
	%	g	%	%	g	g	%	g
ZSM-5	77.4	6.00	81.0	80.0	6.42	6.00	80.0	6.42
PVA	9.0	0.70	5.0	5.0	0.40	0.14	5.0	0.40
SiO_2 (Ludox)	13.6	1.05	14.0	15.0	1.20	1.02	15.0	1.20
Total (dry)	100.0	7.75	100.0	100.0	8.02	7.16	100.0	8.02
H_2O (Ludox)	31.6	2.45	32.6	34.9	2.80	2.39	34.9	2.80
H_2O	6.5	0.50	5.1	0.0	0	0.67	0.0	0
Total (H_2O)	38.1	2.95	37.7	34.9	2.80	3.06	34.9	2.80
Total		10.70			10.82	10.22		10.82

	Trial 7.3		Trial 8.2		Trial 8.3	
	%	g	%	g	%	g
ZSM-5	78.0	6.21	81.2	6.00	84.0	6.20
PVA	5.0	0.40	5.8	0.43	5.0	0.37
SiO_2 (Ludox)	17.0	1.35	13.0	0.96	11.0	0.81
Total (dry)	100.0	7.96	100.0	7.39	100.0	7.38
H_2O (Ludox)	39.6	3.15	30.3	2.24	25.7	1.90
H_2O	0.0	0	6.4	0.47	14.1	1.04
Total (H_2O)	39.6	3.15	36.7	2.71	39.8	2.94
Total		11.11		10.10		10.32

UTSA-16 Extrudates

The extrusion paste is prepared using a mixture of powdered UTSA-16 MOF, PVA as binder and a mixture of water and propanol as plasticizer.

For the preparation of PVA solution, PVA is weighed and immersed in water, stirred at 200 rpm overnight or until the solution is homogenous.

UTSA-16 is weighed, propanol is added and mixed. PVA solution and water are then added in appropriate amounts. Paste is thoroughly blended for 5 - 10 min.

The paste is put through the extruder in open cycle as running circulation mode results in gradual evaporation of propanol and solidification of the mixture inside the extruder. The extrudate is collected and allowed to air-dry before storing.

Note: Attempts to soak the UTSA-16 in excess propanol over a 48-hour period were not successful due to difficulties in controlling the amount adsorbed and, consequently, the variable consistency on the paste.

Figure 13 - Preliminary step: UTSA-16 soaking in propanol.

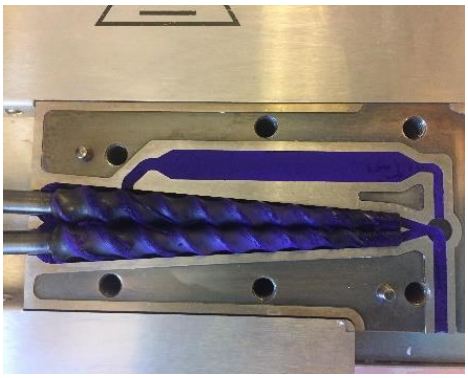

Figure 15 - Extruder compartment following 5 minute, closed-cycle extrusion.

Figure 14 - Extrusion paste.

Figure 16 - Resulting UTSA-16 extrudate.

	Trial 5		Trial 7		Trial 9		Trial 16.2		Trial 16.3	
	%	g	%	g	%	g	%	g	%	g
UTSA-16	97.0	9.40	96.1	10.00	96.2	10.00	97.5	5.00	97.1	5.00
PVA	3.0	0.29	3.9	0.40	3.8	0.39	2.5	0.13	2.9	0.15
Total (dry)	100	9.69	100	10.40	100	10.39	100	5.13	100.0	5.15
H_2O (in PVA)	11.7	1.13	7.7	0.81	7.5	0.78	5.0	0.26	5.8	0.30
H_2O	2.0	0.19	4.9	0.51	5.1	0.53	7.2	0.37	4.9	0.25
Total (H_2O)	13.6	1.32	12.7	1.32	12.6	1.31	12.2	0.63	10.7	0.55
1-PrOH	3.2	0.31	12.6	1.31	12.6	1.31	12.2	0.63	14.2	0.73
Total (liquid)	16.8	1.63	25.2	2.63	25.2	2.62	24.5	1.26	24.9	1.28
Total		11.32		13.03		13.01		6.39		6.43
% 1-PrOH (in liquid)	19.0		49.9		50.0		50.0		57.0	

3.3 Characterization

Every sample prepared was subject to instrumental characterization methods to assess its properties following formulation and evaluate if property deterioration took place. All samples underwent compression tests, scanning electron microscopy and BET surface area assessments. Adsorption equilibrium of pure CH_4, CO_2 and H_2O was measured.

Compression Test

Young's modulus is a mechanical property of solid materials. It measures the stiffness by a defined relation between stress applied in the material and the consequent strain.

To evaluate the stiffness and mechanical stability of the extrudates, 3 pieces of extrudate sample (aprox. 2 mm diameter, 5 mm long) were subjected to compression tests. A Zwick/Roell Z250 universal test machine was equipped with a 500 N load cell for the purpose. Each sample was placed on the centre of the lower compression plate, which was lifted against the upper plate at a rate of 0.5 mm/min. Using the TestXpert II software, a stress-strain curve was plotted with force (N) as function of the sample deformation (mm).

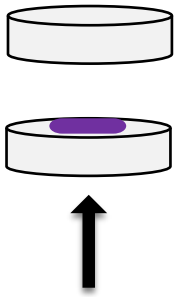

Figure 17 – Diagram of the compression test of a pellet, adapted from [77].

Morphology Analysis with SEM

Scanning electron microscopes (SEM) was used to analyse the morphology of the extrudates, examine their surface and detect any cracks that may have resulted from the drying process. SEM are powerful magnifying instruments with applications in a wide range of research areas. These devices emit a high-energy electron beam over a surface, enabling the observation and characterization of materials on a very small scale. The interaction between the electrons and the sample generates an image of its surface and may disclose information about morphology (texture), composition, crystalline structure and orientation [78].

A Zeiss Auriga CrossBeam FIB/SEM workstation, available at Cenimat/i3N (FCT-UNL), was used to take all SEM images at 5.0 kV acceleration voltage. The extrudates were positioned laying horizontally to expose a flat surface, easing focus.

Surface area assessment

The measurement of the surface area of porous materials is a complex process: while porosity and surface roughness impact the available area, the dimension of the adsorbed molecules influences its determination. The first successful endeavours in surface area determination by gas adsorption were performed in the 1930s by Brunauer and Emmet, leading to the development of the Brunauer-Emmet-Teller (BET) theory in 1938. The BET method has since been applied extensively for gas-solid equilibrium systems. In porous material characterization, it is used for determination of surface area and pore size distribution. Nitrogen (N_2) at liquid temperature (77K) is generally used as adsorptive and the amount adsorbed is evaluated by measurement of gas pressure variation [24].

A BELSORP-mini II instrument was used to obtain N_2 adsorption measurements at 77 K. The first step is activation of the material by heating under vacuum, to ensure the full surface area of the material is available for adsorption. The activation temperature is determined by the properties of the material and their thermal stability. Activation of zeolite extrudates was performed at 773 K overnight followed by 2 hours

at 423 K under vacuum. For MOF extrudates, activation was performed at 393 K for 18 hours, under vacuum.

Following the pre-treatment, an air-tight glass cell containing the sample is flooded with nitrogen at 77K. The measurement follows a discontinuous, point-by-point cycle: increasing amounts of nitrogen are introduced in the sample cell and enough time is allocated for the system to reach equilibrium. The pressure in the sample cell is compared with that of an empty control cell, filled with the same amount of nitrogen at the same temperature. The amount of nitrogen loaded increases gradually until atmospheric pressure is reached.

The formulation of extrudates involved the addition of binders that may block the pores of the material, affecting the porosity. The nitrogen adsorption isotherms allowed measuring the surface area of the formulated materials and control the effect of paste composition on the properties of the material.

3.4 Adsorption equilibrium measurements

The adsorption measurements were performed using volumetric gas adsorption apparatus. The pressure of the studied gas was measured at constant volume and temperature. Inner volume was calibrated before each measurement.

A Belsorp-MAX instrument was used to obtain low pressure adsorption measurements, carried out at 303, 323 and 343 K with CH_4 (purity $>$ 99.995%), CO_2 (purity $>$ 99.9992%) provided by Yara, Norway. Water adsorption measurements were performed at the same temperatures, under pressures of 0 to 4 bar. Activation of zeolite extrudates was performed at 573 K overnight followed by 2 hours at 393 K under vacuum in the Belsorp-MAX instrument. MOF extrudates were activated at 393 K overnight followed by 2 hours at 393 K under vacuum in the Belsorp-MAX instrument. All measurements were performed on the same sample under pressures ranging from 0 to 1 bar. Recording of several adsorption and desorption cycles confirmed that the process is reversible.

The adsorption equilibrium for CH_4 and CO_2 follow a *Type I* isotherm and were fitted to the Langmuir model, which describes adsorption and desorption at identical rates. This is the most basic model for gas-solid adsorption as a monolayer on an ideal surface and the cornerstone of several adsorption theories [21]. The expression used for pure component isotherm is

$$q_A = \frac{q_{A,max}\, K_A p_A}{1 + K_A p_A}$$

where $q_{A,max}$ represents the maximum amount adsorbed of component A and K_A is the adsorption equilibrium constant with exponential dependence on temperature expressed by:

$$K_A = K_A^0 \exp\left(\frac{-\Delta H}{RT}\right)$$

with K_A^0 being the adsorption constant at infinite temperature and $-\Delta H$ as the heat of adsorption.

The adsorption equilibrium for water follows a *Type IV* isotherm, so it cannot be fitted to a Langmuir model.

4. Results and Discussion

4.1 Effect of additives

The additive content greatly affects the consistency of the extrusion paste and its viability to undergo the extrusion process.

In the case of ZSM-5 extrudates, successful extrusion was achieved throughout a wide range of paste compositions. Consequently, extrudates with varied features were obtained. Figure 18 and Figure 19 show the binder composition of the ZSM-5 extrusion pastes and the effect of this composition on extrudate shape and appearance.

The true density of each extrudate sample was calculated by measurement of the mass, length and diameter of each pellet, volume calculation, $V = \pi \frac{d^2}{4} * l$, and application of the density formula, $\rho = \frac{w}{V}$.

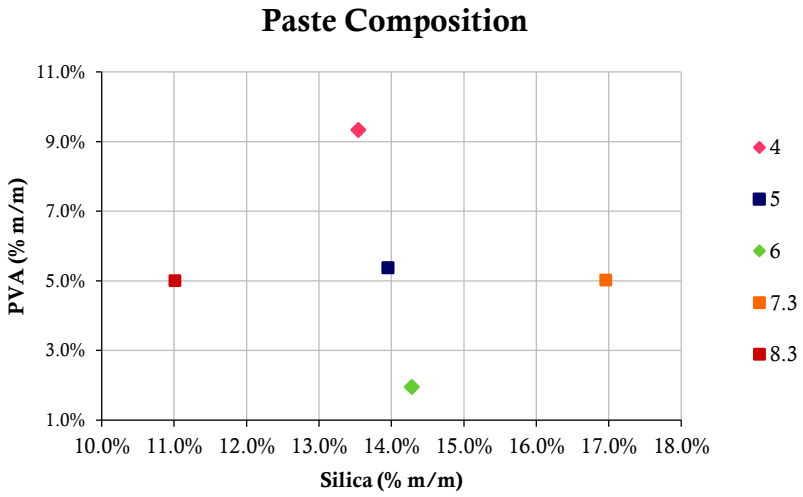

Figure 18 – Graphic representation of binder composition in the ZSM-5 extrusion pastes. ◊ - Open cycle. □ – circulation for 5 minutes.

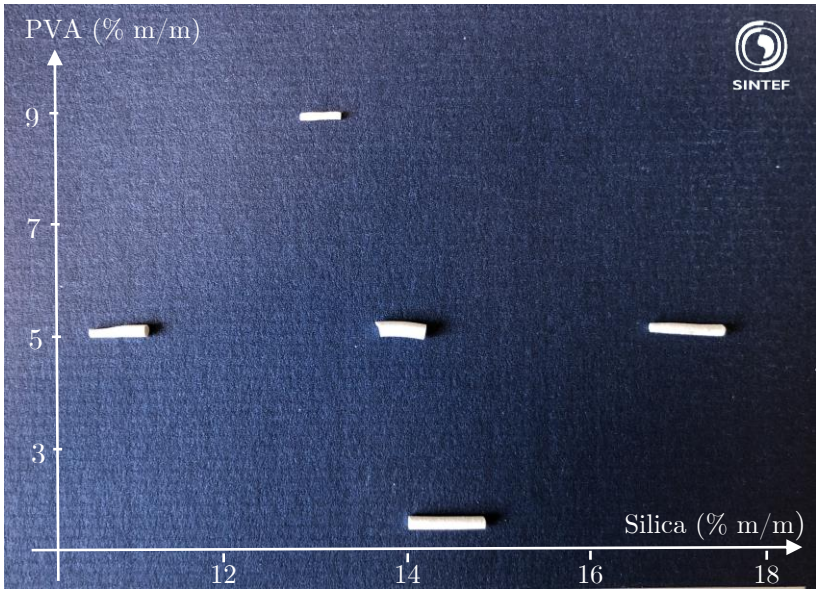

Figure 19 - Effect of binder composition on ZSM-5 extrudates.

Samples 1 to 3 were not extruded successfully.

Sample 4 has high PVA content. The extruded paste was very viscous and flexible resulting, after thermal treatment, in uneven extrudates, with irregular diameter and low mechanical resistance. Extrusion in closed cycle for 5 minutes slightly improved consistency, however these samples weren't selected for further characterization.

Sample 5, with average content, resulted in consistent extrudates. Extrusion in closed cycle for 5 minutes produced stronger extrudates than in open cycle, with true density of 1.17 g/cm^3.

Sample 6 has low PVA content and produced extrudates with regular shape and diameter, with 1.03 g/cm^3 density. This was the only sample in which a 5-minute closed cycle extrusion had detrimental result on the extrudates' quality.

Sample 7, with high silica content, resulted in extrudates with a very irregular surface and slight diameter variations. Closed cycle extrusion resulted in higher viscosity and surface uniformity. Density of 1.13 g/cm^3 was calculated at 15% silica content and 0.98 g/cm^3 at 17%, indicating that the increase past a certain level doesn't improve the extrudate's properties.

Sample 8 has low silica content and resulted in regular shaped extrudates. Extrusion in closed cycle improved surface smoothness and increased viscosity causing greater diameter variations. Density was calculated at 1.14 g/cm^3 for samples with 11% silica and 1.86 g/cm^3 for 13% silica content, representing the highest value obtained, indicative of the ideal composition. Table 5 summarized the results obtained in relation to paste composition.

Table 5 - Relation between composition and extrudate density in ZSM-5 extrudates.

Sample	PVA (wt %)	Silica (wt %)	Density (g/cm^3)
5	5.0	14	1.17
6	2.0	14.3	1.03
7.2	5.0	15.0	1.13
7.3	5.0	17.0	0.98
8.2	5.8	13.0	1.86
8.3	5.0	11.0	1.14

Concerning UTSA-16 crystals, lower susceptibility to composition variations was observed. Successfully extruded MOFs presented similar composition and the small variations produced more uniform samples than in the case of zeolites. The variation in propanol amount had a considerable effect in the resulting amount of extrudate. Figure 20 provides a graphic representation of extrusion paste composition.

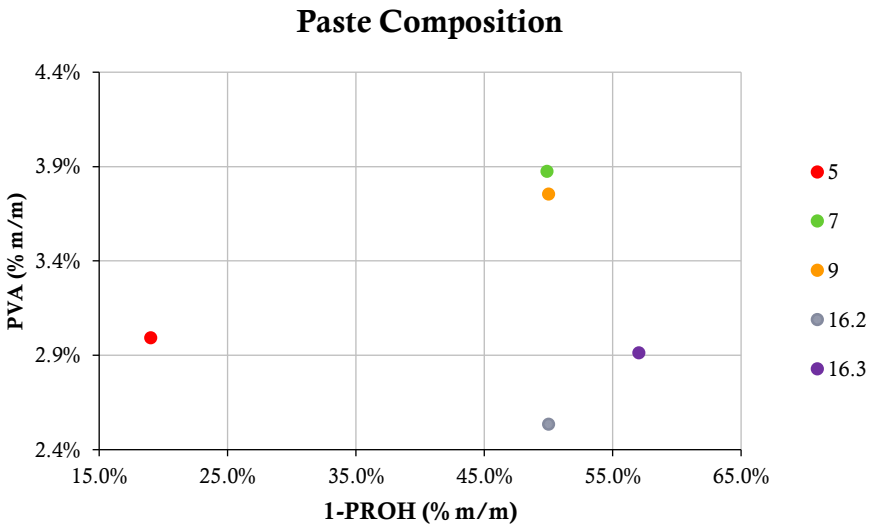

Figure 20 - Graphic representation of PVA and Propanol composition in the UTSA-16 extrusion pastes.

Figure 21 - UTSA-16 extrudates following extrusion and activation.

Samples 1 to 4 were not successfully extruded.

Sample 5 contained a very low amount of propanol, resulting in very limited amount of extrudates, as can be observed in Figure 21. It was verified, however, that the large amount of water used provided this sample with a very uniform surface, and higher density than sample 16.3, with the same amount of PVA and higher propanol content.

Samples 7, 9 and 16.2 were prepared using the same amount of propanol and varying PVA contents. Extrudate density appears to decrease with the increase of PVA content. The extrudate sample with lowest PVA content presented the highest density, at 1.66 g/cm^3.

Table 6 - Relation between composition and extrudate density in UTSA-16 extrudates.

Sample	PVA (wt %)	Propanol (wt % in liquids)	Density
5	3	19	1.58
7	3.9	49.9	1.34
9	3.8	50	1.39
16.2	2.5	50	1.66
16.3	2.9	57	1.37

4.2 SEM Imaging

SEM imaging techniques were used to analyse the morphology of the extrudates and compare them with the pristine powder. Figure 22 and Figure 23 show extrudates with no cracks, uniform surface and regular diameter. A 2 mm die was used for extrusion; the average diameter obtained was 1.88 mm for zeolite pellets and 1.98 mm for MOF pellets. In Figure 22 it is possible to observe a flat area in one of the sides of the ZSM-5 extrudate sample. This deformation occurred as the material was placed on a flat surface to dry following extrusion; the slightly viscous nature of the fresh sample caused it to mould to the surface.

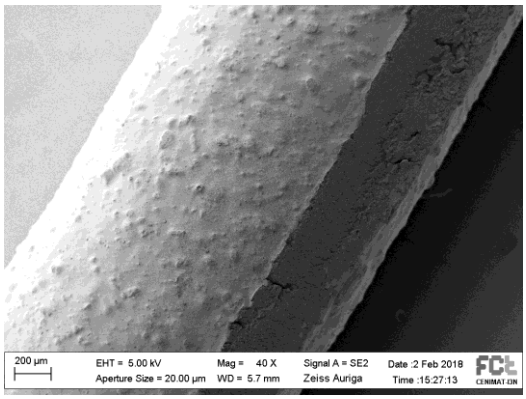

Figure 22 - ZSM-5 extrudate, sample 8.3.

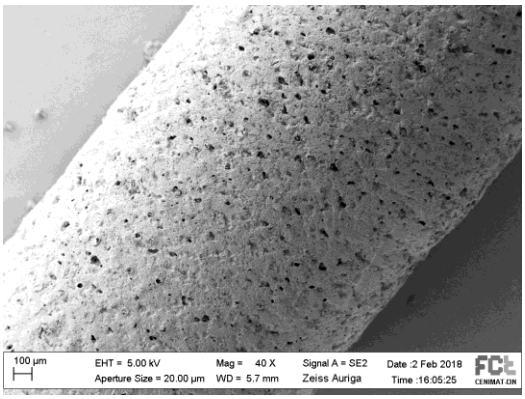

Figure 23 - UTSA-16 extrudate, sample 9.

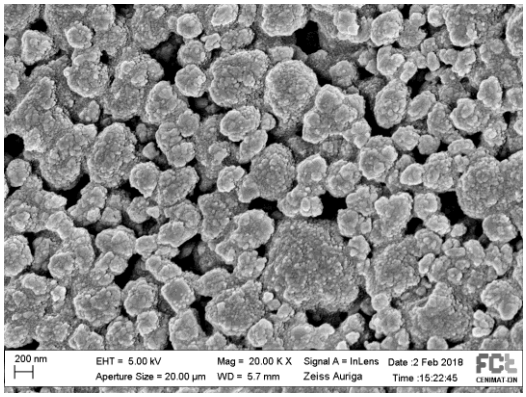

Figure 24 - ZSM-5 extrudate surface.

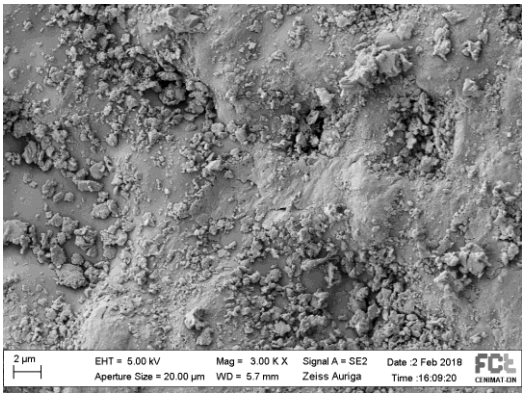

Figure 25 - UTSA-16 extrudate surface.

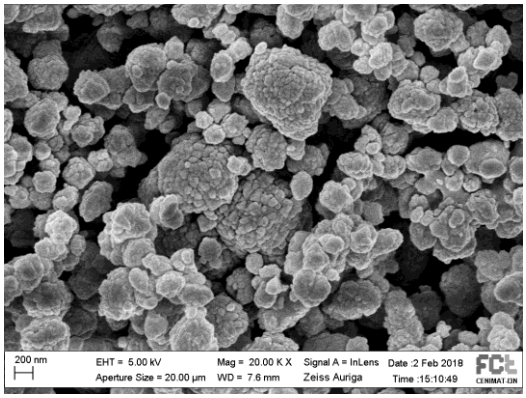

Figure 26 - Powdered ZSM-5.

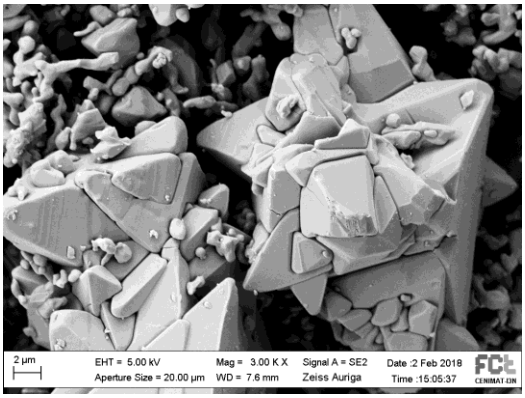

Figure 27 - Powdered UTSA-16.

The comparison of the surfaces of extrudates with the imaging of the pristine powder before any alteration, shows how the extrusion process affected the surface of the materials. In the case of ZSM-5, the comparison of Figure 24 and Figure 26 makes it clear that the material underwent extrusion without suffering deformation. The crystal structure remains almost unchanged, although it is possible to observe a tighter crystal packing in the extrudate and predominance of smaller and more homogenous structures, with sizes of 200 to 500 nm. Silica particles are too small to be distinguishable. In the case of the UTSA-16 extrudates, a much larger variation is observable between Figure 25 and Figure 27, due to the MOF lower stability and resistance to pressure. While the powdered material originally presented complex crystal structures of very large dimensions, the high shear forces it was exposed to during extrusion appears to have caused damage to the crystalline structure. The extrudates present a mostly smooth surface with small irregularities throughout.

4.3 Mechanical strength

The mechanical stability of the extrudates was assessed by exposing pellets from different samples to crush tests. Three repetitions were performed for each sample, using one single pellet for each. Examples of test results for each material are shown on Figure 28 and Figure 29.

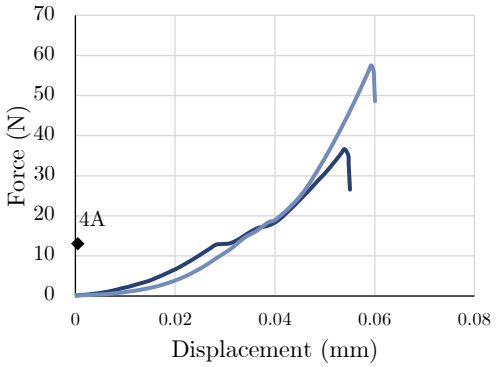

Figure 28 - Compression test results, two pellets of the same ZSM-5 extrudate sample. (Commercial 4A zeolite extrudate reported result for comparison [71]).

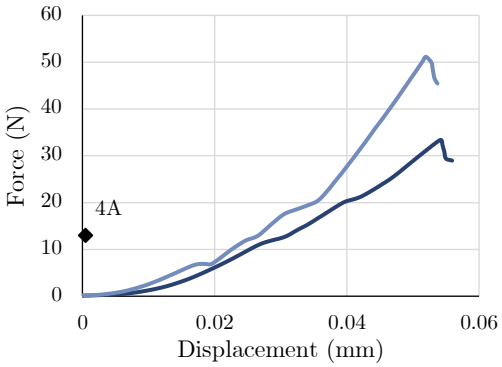

Figure 29 - Compression test results, two pellets of the same UTSA-16 extrudate sample. (Commercial 4A zeolite extrudate reported result for comparison [71]).

There seems to be a correlation between silica content and hardness in ZSM-5 extrudates, shown in Figure 30, although at high silica concentrations the material's resistance drops. Irregular surface and diameter variations observed in samples with high silica content may explain this behaviour. Only silica content is analysed as PVA is expected to be removed from ZSM-5 extrudates. The results obtained for UTSA-16 extrudates seem to indicate that the hardness of the material would decrease as binder content increases, as shown in Figure 31. This inference is opposite to what is reported in previous studies [71], [79], where the binder content was reported to have a positive effect on the mechanical strength of the material.

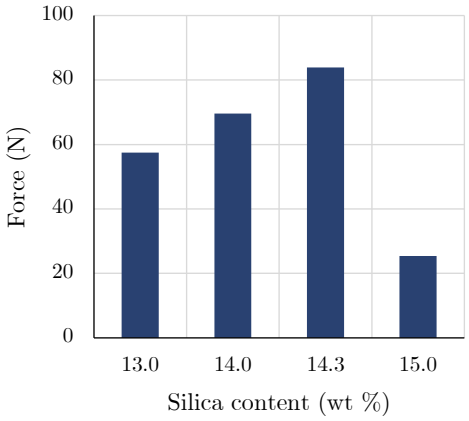

Figure 30 – Force applied on ZSM-5 extrudates in relation to Silica content.

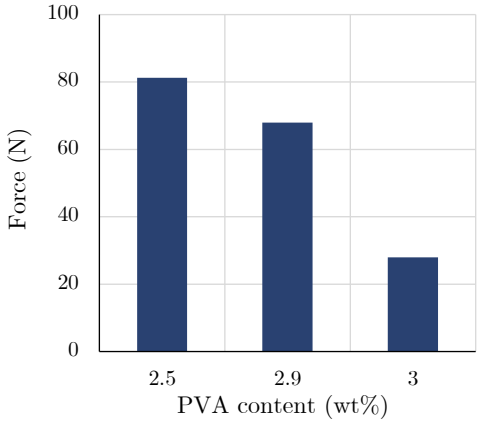

Figure 31 – Force applied on UTSA-16 extrudates in relation to PVA content.

Another study, analyses the mechanical strength in MOF-5 pellets as a function of density, observing that as density increases, so does the pellet's resistance [80]. However, in this case, the ZSM-5 extrudates do not follow the relation described (Figure 32). At the UTSA-16 extrudates the denser samples are considerably more resistant than the least dense one (Figure 33).

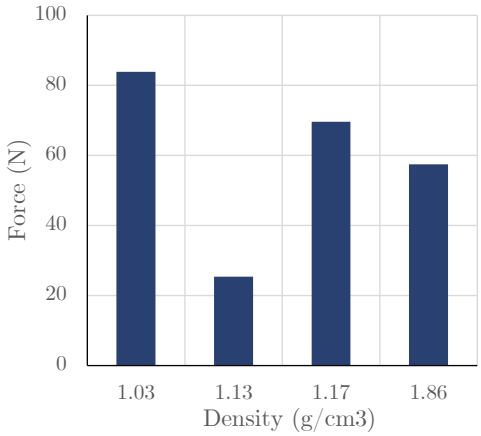

Figure 32 – Force applied on ZSM-5 extrudates in relation to sample density.

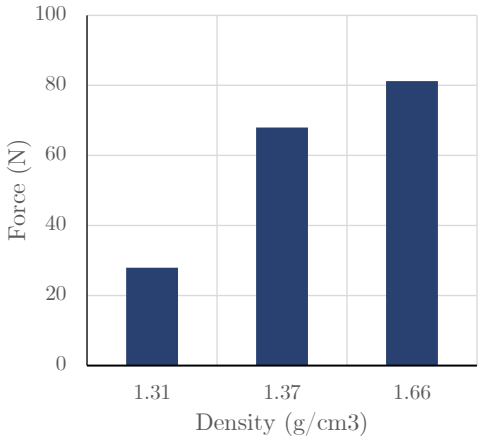

Figure 33 - Force applied on UTSA-16 extrudates in relation to binder content.

4.4 Surface area

The N_2 adsorption isotherms for determination of surface area and micropore volume are shown on Figure 34 and Figure 35,for zeolite and MOF pellets, respectively.

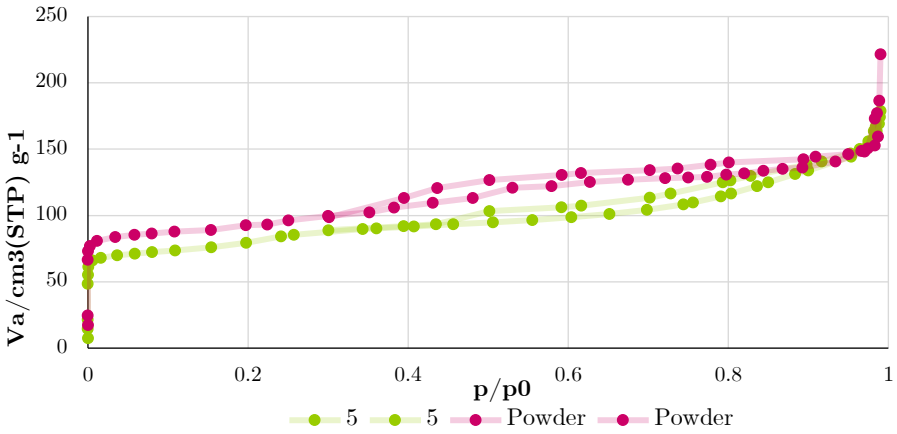

Figure 34 - N2 adsorption isotherms at 77 K for ZSM-5 powder and extrudate.

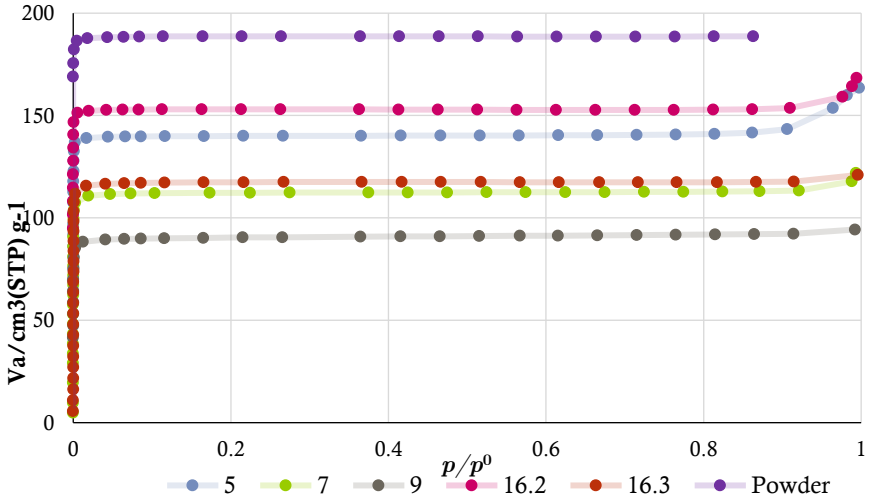

Figure 35 – N_2 adsorption isotherms at 77 K for UTSA-16 extrudates and powder.

All extrudates display a *type I* isotherm indicative of a microporous sample with pore filling at high relative pressures.

In the case of zeolite extrudates, an average 9% decrease was observed in relation to the original BET surface area, with 7% reduction in the best samples. In metal-organic framework extrudates, the PVA is not removed from the extrudates because activation is performed at lower temperatures. An average decrease of 38% in the BET surface area was observed in these extrudates, with 22% reduction on the best sample.

The textural results obtained for the best extrudate formulations are summarized in Table 7.

Table 7 - Textural results for best formulation compositions.

Porous Material	BET area (m^2/g)	Micropore volume (cm^3/g)	Mean pore diameter (nm)
ZSM-5	318	0.260	3.27
UTSA-16	651	0.256	1.57

Increasing amounts of binders should cause a decrease in the surface area of extrudates. Figure 36 and Figure 37 show the loss of surface area in relation to the samples' binder content.

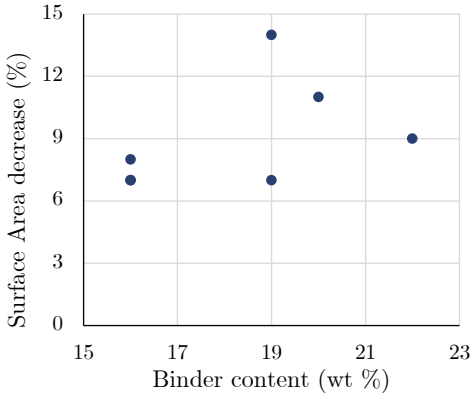

Figure 36 - Surface area decrease in relation to the pristine powder as function of the binder content, activation at 773K.

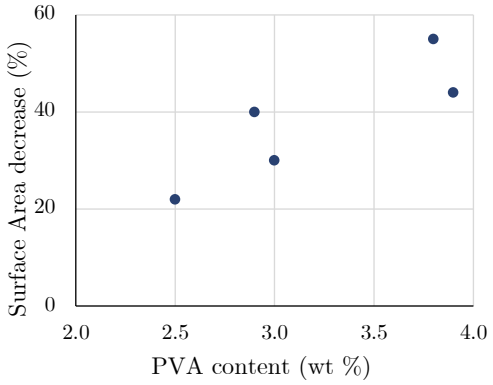

Figure 37 – Surface area decrease in relation to the pristine powder as function of the binder content, activation at 393K.

A correlation doesn't seem to exist between silica content and surface area in ZSM-5 extrudates. This may happen because, despite causing pore blockage within the zeolite, silica is porous itself. A direct relation is observable between binder content and surface area reduction for UTSA-16 extrudates. This observation is in agreeance with previous studies [71], where pore blockage by the large dimension binder molecules was highlighted as a possible cause for surface area reduction.

4.5 Adsorption

The adsorption equilibrium measurements for CH_4, CO_2 and H_2O on ZSM-5 extrudates are shown in Figure 38 to Figure 42. The same measurements on UTSA-16 extrudates are shown in Figure 43 to Figure 47.

The Langmuir model was used for the fitting of CH4 and CO2 samples, providing an adequate fit to the experimental data. Model parameters are listed on Table 8.

The H_2O adsorption equilibrium isotherms do not follow a *Type I* shape and, therefore cannot be fitted using the Langmuir model. These isotherms have not been modelled.

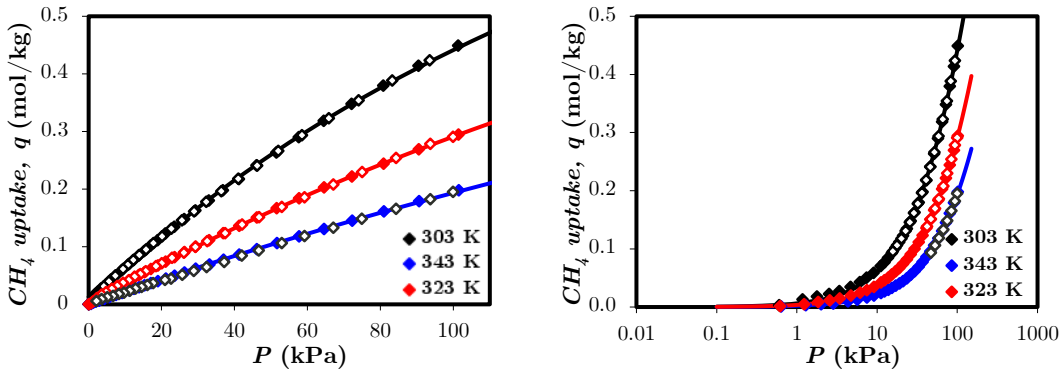

Figure 38 - Adsorption equilibrium of CH_4 on ZSM-5 extrudates at 303, 323, and 343 K. The filled symbols denote adsorption data and open symbols denote desorption data. Solid lines are fittings from the Langmuir isotherm.

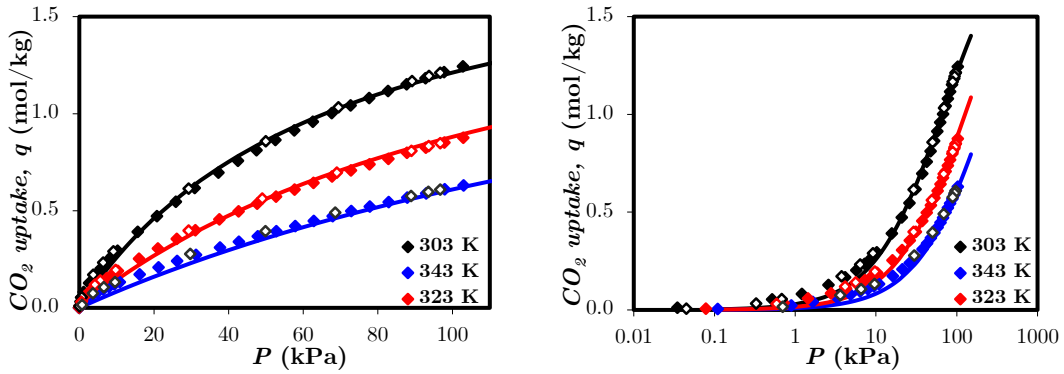

Figure 39 - Adsorption equilibrium of CO_2 on ZSM-5 extrudates at 303, 323, and 343 K. The filled symbols denote adsorption data and open symbols denote desorption data. Solid lines are fittings from the Langmuir isotherm.

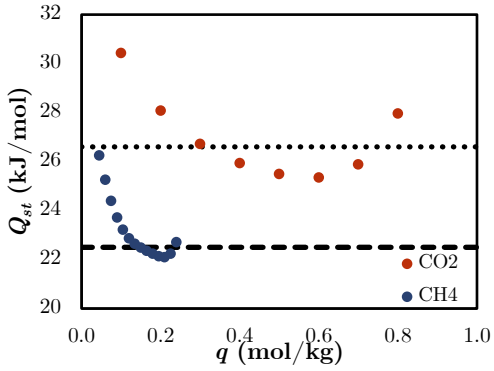

Figure 40 – Isosteric heat as a function of loading. Dashed lines represent the ΔH parameter employed in the Langmuir fitting.

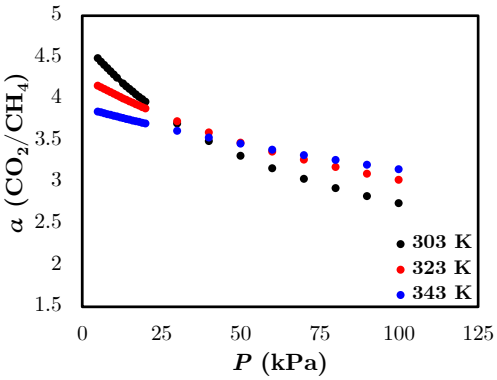

Figure 41 – CO_2/CH_4 selectivity as a function of pressure.

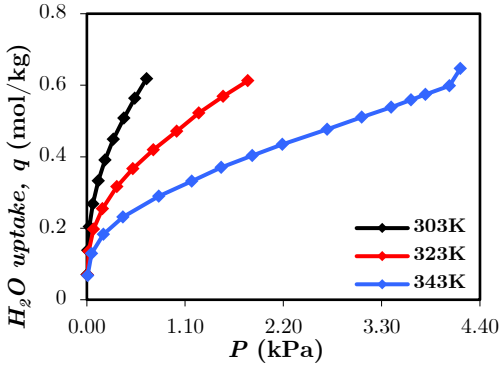

Figure 42 – Adsorption equilibrium of H_2O on ZSM-5 extrudates at 303, 323, and 343 K, not modelled.

Figure 1 and 2 present the adsorption equilibria of CH_4 and CO_2 on ZSM-5 at 303, 323, and 343 K within 0 to 100 kPa. The isotherms shape are *Type I* and the results presented show that the experimental data is successfully fitted with the Langmuir model. The results obtained for each adsorbate in ZSM-5 extrudates are in good agreement with data reported in the literature [81], [82]. The high silica content within these extrudates explains the adsorption of higher quantities of methane and lower quantities of water when compared with previous studies.

Figure 3 shows the isosteric heats of adsorption for CO_2 and CH_4 as a function of the respective loadings. The horizontal dashed lines represent, the adsorption heat used as parameter for the Langmuir model curve fitting. The study of isosteric heat confirms the occurrence of physisorption in both modelled cases (Qst $<$ 80kJ/mol). The adsorption of carbon dioxide involves higher interaction energy than methane. Although both components show variation of isosteric heat with loading, indicative of energetically heterogenous behaviour, methane presents a considerable wider variation with loading. Nevertheless, the results presented in Figure 40 show that the ΔH parameter employed in the Langmuir fitting (dashed lines), reported in Table 8, is in accordance with the calculated isosteric heats of adsorption.

Figure 4 presents the CO_2/CH_4 equilibrium selectivity. The study of selectivity, made by comparison of adsorption capacities of CO2 and CH4 under the same pressure and temperature, shows the extrudates hold higher affinity to CO_2 than CH_4. This feature seems to be highly dependent on pressure, decreasing significantly as pressure increases. Figure 5 presents the adsorption equilibria of water vapour on ZSM-5 extrudates at 303, 323, and 343 K. Previous studies report that the saturation concentration of water in ZSM-5 presents significant variation in connection with Si/Al ratios and the presence of defects within the porous material [83], [84]. For this reason, due to the high Si/Al ratio in the ZSM-5 extrudates a lower H_2O uptake was obtained, in comparison with the literature.

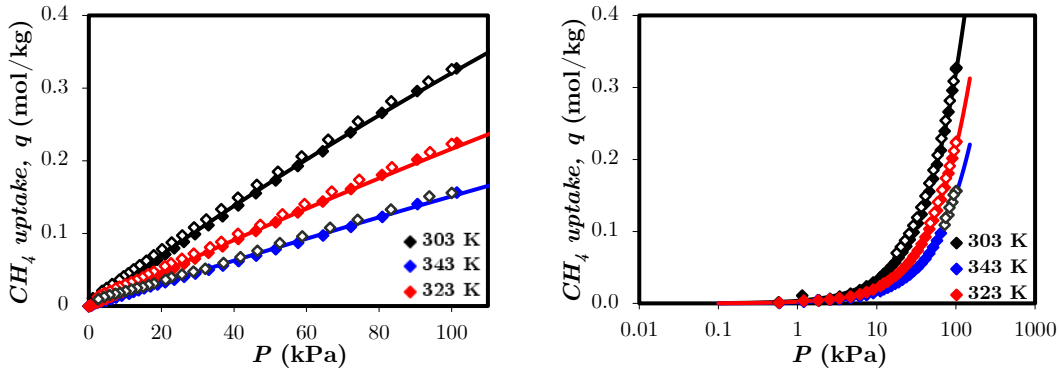

Figure 43 – Adsorption equilibrium of CH_4 on UTSA-16 extrudates at 303, 323, and 343 K. The filled symbols denote adsorption data and open symbols denote desorption data. Solid lines are fittings from the Langmuir isotherm.

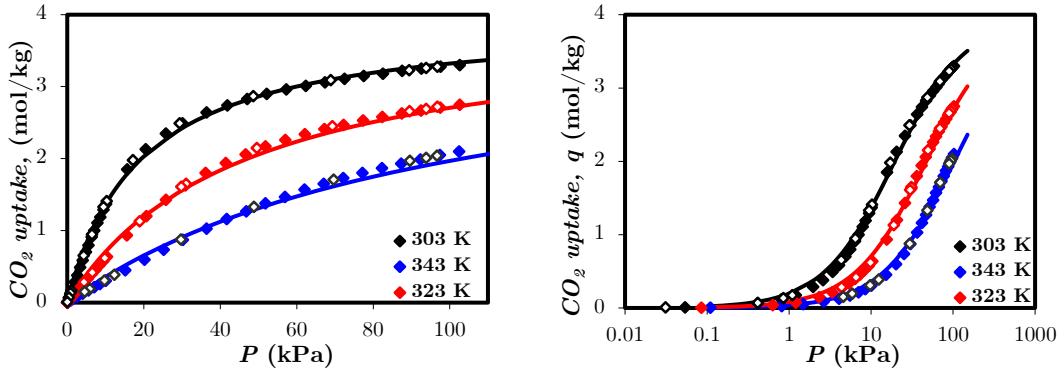

Figure 44 – Adsorption equilibrium of CO_2, on UTSA-16 extrudates at 303, 323, and 343 K. The filled symbols denote adsorption data and open symbols denote desorption data. Solid lines are fittings from the Langmuir isotherm..

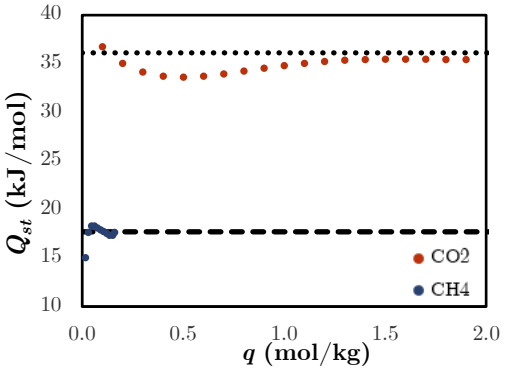

Figure 45 - Isosteric heat as a function of loading. Dashed lines represent the ΔH parameter employed in the Langmuir fitting.

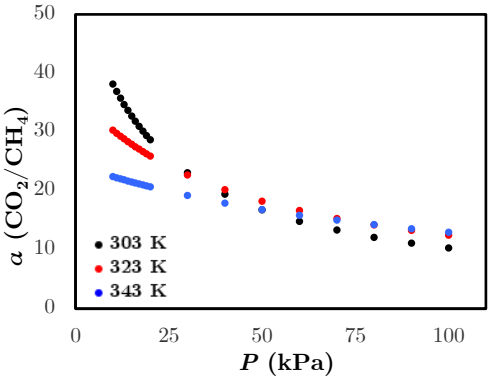

Figure 46 - CO_2/CH_4 selectivity as a function of pressure.

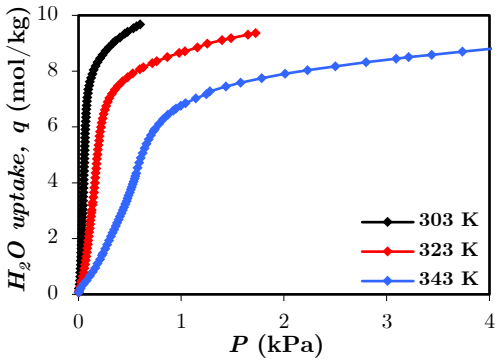

Figure 47 - Adsorption equilibrium of H_2O on UTSA-16 extrudates at 303, 323, and 343 K, not modelled.

Figure 6 and 7 present the adsorption equilibria of CH_4 and CO_2 on UTSA-16 at 303, 323, and 343 K within 0 to 100 kPa. The isotherms shape are *Type I* and the results presented show that the experimental data is successfully fitted with the Langmuir model. The values obtained in UTSA-16 adsorption are somewhat lower than those reported in the literature [71]. This is expectable, considering the lower surface areas in these extrudates.

Figure 8 shows the isosteric heats of adsorption for CO_2 and CH_4 on UTSA-16 as a function of the respective loadings. The occurrence of physisorption in the modelled cases is once again confirmed by the analysis of isosteric heats ($Q_{st} < 80$kJ/mol). In UTSA-16, the adsorption of carbon dioxide also involves higher interaction energy than methane. In this case, the isosteric heat seems to be independent of loading in both cases, indicating energetically homogenous behaviour. Once again, the calculated heats of adsorption are in accordance with the Langmuir fitting parameter (ΔH), as reported in Table 8.

Figure 9 shows the CO_2/CH_4 equilibrium selectivity as a function of pressure at 303, 323, and 343 K. The study of selectivity shows the extrudates hold very high affinity to CO_2 (about 10 times as high as observed on ZSM-5 extrudates). Again, this feature seems to be highly dependent on pressure, decreasing considerably as it increases. Zeolite extrudates show slightly higher capacity for methane adsorption than UTSA-16 extrudates. The opposite is observed for CO2 adsorption, where UTSA-16 pellets show nearly twice as much capacity than ZSM-5 extrudates. This justifies the much higher CO_2/CH_4 selectivity observed for the MOF.

Figure 10 presents the adsorption equilibria of water vapour on UTSA-16 extrudates at 303, 323, and 343 K. The isotherms shape corresponds to *Type V* of the IUPAC classification and, therefore, could not be fitted with the Langmuir model. The obtained results show that UTSA-16 adsorbs more than 10 times the amount of water adsorbed by the high Si/Al ratio ZSM-5 extrudates produced.

Table 8 - Langmuir parameters of CH4 and CO2 adsorption on ZSM-5 and UTSA-16 extrudates.

	CH_4	CO_2
ZSM-5 extrudates		
$q_{A,max}$, mol/kg	1.50	2.0
$K_A{}^0$, kPa^{-1}	$5.7x10^{-7}$	$3.8x10^{-7}$
$-\Delta H$, J/mol	22500	26600
UTSA extrudates		
$q_{A,max}$, mol/kg	2.8	4.0
$K_A{}^0$, kPa^{-1}	$1.2x10^{-6}$	$3.2x10^{-8}$
$-\Delta H$, J/mol	17700	36120

5. Conclusions and Further Work

This study was focused on the formulation of porous materials and their characterization, with measurement of adsorption equilibrium for methane and carbon dioxide to evaluate the viability of the application of these materials for natural gas or biogas capture. Additionally, water adsorption was evaluated to evaluate material stability and moisture resistance.

Zeolite (ZSM-5) and metal-organic framework (UTSA-16) pellets were formulated by extrusion, in an established four-step. Pre-existent paste compositions were adapted and variations were made to evaluate the effect of varying additive composition on the extrudate properties. In the case of ZSM-5 extrudates, the commonly used alumina binder was replaced with colloidal silica, which increase the material's selectivity to methane adsorption.

The formulation process resulted in pellets of uniform surface and diameter, without cracks. A surface area reduction was observed in zeolite samples (9% average decrease) and more significant decrease in MOF extrudates (38% average decrease), due to considerable collapse of the crystalline structure subject to high shear forces during the extrusion process and some degree of pore blocking caused by the binder molecules. It was observed that lower binder content originates denser pellets. The density of ZSM-5 extrudates (1.19 g/cm^3, average) was similar to commercial zeolite pellets. In UTSA-16 it was considerably superior (1.47 g/cm^3, average). Increasing silica content to a certain level in zeolites led to growing mechanical strength of the extrudates. The opposite was observed in MOF extrudates, which is contrary to previously reported results. The mechanical strength obtained for the majority of samples was considerably higher than reported for commercial zeolite pellets.

Both extrudates were shown to adsorb methane and carbon dioxide at rates similar to those described in the literature. Slightly higher amounts of methane were adsorbed on ZSM-5 extrudates than what is described in previous studies, likely due to the larger silica ratio existing in these pellets. Additionally, ZSM-5 extrudates showed considerably low affinity to water, a desirable feature that can be explored for several applications. UTSA-16 extrudates show higher capacity for carbon dioxide adsorption, adsorbing nearly twice as much as ZSM-5 extrudates. The formulation processes implemented yielded favorable results, particularly for ZSM-5 extrudates. Both materials showed viability for application in natural gas or biogas storage.

Future research in formulation should be focused on process optimization, namely the prevention of crystal structure collapse and pore blocking. Regarding adsorption selectivity, it would be interesting to evaluate adsorption at higher pressures. In addition, the study of separation efficiency for binary mixes, like CH_4/CO_2 would

provide further insight into the suitability of these materials for gas separation and storage.

6. References

[1] British Petroleum, "BP Statistical Review of World Energy 2017," *Br. Pet.*, no. 66, pp. 1–52, 2017.

[2] Center for climate and energy solutions C2ES, "Leveraging Natural Gas to Reduce Greenhouse Gas Emissions," no. June, p. 116, 2013.

[3] C. Solar, A. G. Blanco, A. Vallone, and K. Sapag, *Adsorption of Methane in Porous Materials as the Basis for the Storage of Natural Gas*, no. Natural Gas. Sciyo, 2010.

[4] J. P. B. Mota, "Impact of Gas Composition on Natural Gas Storage by Adsorption," *AIChE J.*, vol. 45, no. 5, pp. 986–996, 1999.

[5] S. Cavenati, C. A. Grande, A. E. Rodrigues, C. Kiener, and U. Müller, "Metal organic framework adsorbent for biogas upgrading," *Ind. Eng. Chem. Res.*, vol. 47, no. 16, pp. 6333–6335, 2008.

[6] M. Hagen, E. Polman, J. K. Jensen, A. Myken, O. Jonsson, and A. Dahl, "Report SGC 118 - Adding gas from biomass to the gas grid," *Swedish Gas Cent.*, no. July, 2001.

[7] Basic Energy Sciences Workshop, "Basic Research Needs for Carbon Capture: Beyond 2020," pp. 1–196, 2010.

[8] S. Sircar, "Applications of gas separation by adsorption for the future," *Adsorpt. Sci. Technol.*, vol. 19, no. 5, pp. 347–366, 2001.

[9] R. A. Munson and R. A. J. Clifton, "Natural Gas Storage With Zeolites," 1971.

[10] J. A. Mason, M. Veenstra, and J. R. Long, "Evaluating Metal–Organic Frameworks for Natural Gas Storage.," *Chem. Sci.*, vol. 5, no. 1, pp. 32–51, 2014.

[11] J. Li *et al.*, "Carbon dioxide capture-related gas adsorption and separation in metal-organic frameworks," *Coord. Chem. Rev.*, vol. 255, no. 15–16, pp. 1791–1823, 2011.

[12] A. G. Slater and A. I. Cooper, "Funtion-led design of new porous materials," *Science (80-.).*, vol. 348, no. 6338, 2015.

[13] J. Li, R. J. Kuppler, and H. Zhou, "Selective gas adsorption and separation in metal – organic frameworks," *Chem. Soc. Rev.*, vol. 38, pp. 1477–1504, 2009.

[14] F. Rezaei and P. Webley, "Structured Adsorbents in Gas Separation Processes," *Sep. Purif. Technol.*, vol. 70, pp. 243–256, 2010.

[15] D. Crawford, J. Casaban, R. Haydon, N. Giri, T. Mcnally, and S. L. James, "Synthesis by extrusion: continuous, large-scale preparation of MOFs using little or no solvent," *Chem. Sci.*, vol. 6, no. 3, pp. 1645–1649, 2015.

[16] J. G. Calvert, "Glossary of atmospheric chemistry terms," *Pure Appl. Chem.*, vol. 62, no. 11, pp. 2167–2219, 1990.

[17] M. Suzuki, *Adsorption engineering*, vol. 14. Tokyo: Kodansha Ltd. and Elsevier Science Publishers, 1990.

[18] J. U. Keller and R. Staudt, *Gas adsorption equilibria: Experimental methods and adsorptive isotherms*. Boston: Springer Science, 2005.

[19] D. Ruthven, S. Farooq, and K. Knaebel, "Pressure Swing Adsorption." p. 352, 1993.

[20] R. T. Yang, *Gas Separation by Adsorption Processes*. 1987.

[21] D. D. Do, *Adsorption Analysis: Equilibria and Kinetics*, vol. 2. 1998.

[22] D. M. Ruthven, *Principles of Adsorption and Adsorption Processes*. John Wiley & Sons, Inc., 1984.

[23] A. W. Adamson and A. P. Gast, *Physical Chemistry of Surfaces*, 6th ed. John Wiley & Sons, Inc., 1997.

[24] F. Rouquerol, J. Rouquerol, K. S. W. Sing, P. Llewellyn, and G. Maurin, *Adsorption by Powders and Porous Solids*, Second Edi. Academic Press, Elsevier, 2014.

[25] M. Thommes *et al.*, "Physisorption of gases, with special reference to the evaluation of surface area and pore size distribution (IUPAC Technical Report)," *Pure Appl. Chem.*, vol. 87, no. 9–10, pp. 1051–1069, 2015.

[26] A. Dabrowski, "Adsorption - From Theory to Practice," *Adv. Colloid Interface Sci.*, vol. 93, no. 1–3, pp. 135–224, 2001.

[27] K. S. W. Sing *et al.*, "Reporting Physisorption Data for Gas/Solid Systems," *Pure Appl. Chem.*, vol. 57, no. 4, pp. 603–619, 1985.

[28] A. Schoedel, Z. Ji, and O. M. Yaghi, "The role of metal-organic frameworks in a carbon-neutral energy cycle," *Nat. Energy*, no. April, pp. 1–13, 2016.

[29] H. Furukawa *et al.*, "Water Adsorption in Porous Metal-Organic Frameworks and Related Materials," *J. Am. Chem. Soc.*, vol. 136, pp. 4369–4381, 2014.

[30] X.-Y. Yang, L.-H. Chen, Y. Li, J. C. Rooke, C. Sanchez, and B.-L. Su, "Hierarchically Porous Materials: synthesis strategies and structure design," *Chem. Soc. Rev.*, vol. 46, no. 2, pp. 481–558, 2017.

[31] R. M. Milton, *Molecular Sieve Science and Technology*, no. 1. 1989.

[32] R. M. Milton, "Molecular sieve adsorbents," U.S. 2882243, 1959.

[33] D. W. Breck, W. G. Eversole, and R. M. Milton, "New Synthetic Crystalline Zeolites," *J. Am. Chem. Soc.*, vol. 78, no. 10, pp. 2338–2339, 1956.

[34] L. B. McCusker, D. H. Olson, and C. Baerlocher, *Atlas of Zeolite Framework Types*, Sixth Revi. Elsevier, 2007.

[35] H. van Koningsveld, J. C. Jansen, and H. van Bekkum, "The monoclinic framework structure of zeolite H-ZSM-5. Comparison with the orthorhombic framework of as-synthesized ZSM-5," *Zeolites*, vol. 10, no. 4, pp. 235–242, 1994.

[36] S. M. Auerbach, K. A. Carrado, and P. K. Dutta, *Handbook of Zeolite Science and Technology*. Macel Dekker, Inc., 2003.

[37] D. H. Olson, G. T. Kokotailo, S. L. Lawton, and W. M. Meier, "Crystal Structure and Structure-Related Properties of ZSM-5," *J. Phys. Chem.*, vol. 85, no. 15, pp. 2238–2243, 1981.

[38] A. Masala *et al.*, "Conductive ZSM-5-Based Adsorbent for CO2Capture: Active Phase vs Monolith," *Ind. Eng. Chem. Res.*, vol. 56, no. 30, pp. 8485–8498, 2017.

[39] H. Furukawa *et al.*, "Ultrahigh Porosity in Metal-Organic Frameworks," *Science (80-.).*, vol. 329, pp. 424–428, 2010.

[40] O. K. Farha *et al.*, "Metal-organic Framework Materials with Ultrahigh Surface Areas: Is the Sky the Limit?," *J. Am. Chem. Soc.*, vol. 134, no. 36, pp. 15016–15021, 2012.

[41] W. Y. Hong, S. P. Perera, and A. D. Burrows, "Manufacturing of metal-organic framework monoliths and their application in CO 2 adsorption," *Microporous Mesoporous Mater.*, vol. 214, pp. 149–155, 2015.

[42] J. Ren, H. W. Langmi, B. C. North, and M. Mathe, "Review on processing of metal – organic framework (MOF) materials towards system integration for hydrogen storage," *Int. J. Energy Res.*, vol. 39, no. 5, pp. 607–620, 2015.

[43] J. Lee, O. K. Farha, J. Roberts, K. A. Scheidt, S. T. Nguyen, and J. T. Hupp, "Metal – organic framework materials as catalysts," *Chem. Soc. Rev.*, vol. 38, no. 5, pp. 1450–1459, 2009.

[44] F. X. L. i Xamena and J. Gascon, *Metal Organic Frameworks as Heterogenous Catalysts*. Royal Society of Chemistry, 2013.

[45] I. Stassen, N. Burtch, A. Talin, P. Falcaro, M. Allendorf, and R. Ameloot, "An Updated Roadmap for the Integration of Metal-Organic Frameworks with Electronic Devices and Chemical Sensors," *Chem. Soc. Rev.*, vol. 46, pp. 3185–3241, 2017.

[46] L. Wang, Y. Han, X. Feng, J. Zhou, P. Qi, and B. Wang, "Metal–Organic Frameworks for Energy Storage: Batteries and Supercapacitors," *Coord. Chem. Rev.*, vol. 307, pp. 361–381, 2016.

[47] M. D. Allendorf, C. A. Bauer, R. K. Bhakta, and R. J. T. Houk, "Luminescent Metal-Organic Frameworks," *Chem. Soc. Rev.*, no. 38, pp. 1330–1352, 2009.

[48] Y. Kinoshita, I. Matsubara, T. Higuchi, and Y. Saito, "The Crystal Structure of Bis(adiponitrilo)copper(I) Nitrate," *Bull. Chem. Soc. Jpn.*, vol. 32, no. 11, pp. 1221–1226, 1959.

[49] F. W. Knobloch and W. H. Rauscher, "Coordination Polymers of Copper(II) Prepared A t Liquid-Liquid Interfaces," *J. Polym. Sci.*, vol. 38, no. 133, pp. 261–262, 1959.

[50] B. P. Block, E. S. Roth, C. W. Schaumann, J. Simkin, S. Rose, and H., "Coordination Polymers with Inorganic Backbones Formed by Double-Bridging of Tetrahedral Elements," *J. Am. Chem. Soc.*, vol. 84, pp. 3200–3201, 1962.

[51] B. F. Hoskins and R. Robson, "Design and Construction of a New Class of Scaffolding-like Materials Comprising Infinite Molecular Rods.," *J. Am. Chem. Soc.*, vol. 112, p. 1546, 1990.

[52] S. Kitagawa, S. Matsuyama, M. M., and T. Emori, "Synthesis and Crystal Structures of Novel One-dimensional Polymers," *J. Chem. Soc. Dalt. Trans.*, no. 11, pp. 2869–2874, 1991.

[53] O. M. Yaghi and H. Li, "Hydrothermal Synthesis of a Metal-Organic Framework Containing Large Rectangular Channels," *J. Am. Chem. Soc.*, vol. 117, pp. 10401–10402, 1995.

[54] D. Riou, O. Roubeau, and G. Férey, "Composite microporous compounds, Part I.," *Microporous Mesoporous Mater.*, vol. 23, no. 1–2, pp. 23–31, 1998.

[55] P. Z. Moghadam *et al.*, "Development of a Cambridge Structural Database Subset: A Collection of Metal − Organic Frameworks for Past, Present, and Future," *Chem. Mater.*, vol. 29, no. 7, pp. 2618–2625, 2017.

[56] O. K. Farha and J. T. Hupp, "Rational Design, Synthesis, Purification and Activation of Metal - Organic Framework Materials," *Acc. Chem. Res.*, vol. 43, no. 8, pp. 1166–1175, 2010.

[57] S. Furukawa, J. Reboul, S. Diring, K. Sumida, and S. Kitawaga, "Structuring of metal – organic frameworks at the mesoscopic / macroscopic scale," *Chem. Soc. Rev.*, vol. 43, pp. 5700–5734, 2014.

[58] M. Fernandez, T. K. Woo, C. E. Wilmer, and R. Q. Snurr, "Large-Scale Quantitative Structure−Property Relationship (QSPR) Analysis of Methane Storage in Metal−Organic Frameworks," *J. Phys. Chem. C*, no. 117, pp. 7681–7689, 2013.

[59] F. X. Coudert, "Responsive metal-organic frameworks and framework materials:

Under pressure, taking the heat, in the spotlight, with friends," *Chem. Mater.*, vol. 27, no. 6, pp. 1905–1916, 2015.

[60] S. Xiang, X. Wu, J. Zhang, R. Fu, S. Hu, and X. Zhang, "A 3D Canted Antiferromagnetic Porous Metal-Organic Framework with Anatase Topology through Assembly of an Analogue of Polyoxometalate," *J. Am. Chem. Soc.*, vol. 127, no. 47, pp. 16352–16353, 2005.

[61] A. Masala, J. G. Vitillo, F. Bonino, M. Manzoli, C. A. Grande, and S. Bordiga, "New insights into UTSA-16," *Phys. Chem. Chem. Phys.*, vol. 18, no. 1, pp. 220–227, 2016.

[62] S. Xiang *et al.*, "Microporous metal-organic framework with potential for carbon dioxide capture at ambient conditions," *Nat. Commun.*, vol. 3, p. 954, 2012.

[63] V. I. Agueda *et al.*, "Adsorption and diffusion of H2, N2, CO, CH4 and CO2 in UTSA-16 metal-organic framework extrudates," *Chem. Eng. Sci.*, vol. 124, pp. 159–169, 2015.

[64] F. Rezaei and P. Webley, "Optimum structured adsorbents for gas separation processes," *Chem. Eng. Sci.*, vol. 64, no. 24, pp. 5182–5191, 2009.

[65] S. Mitchell, N. Michels, and J. Pe, "From Powder to Technical Body: the undervalued science of catalyst scale up," *Chem. Soc. Rev.*, vol. 42, pp. 6094–6112, 2013.

[66] F. Akhtar, L. Andersson, S. Ogunwumi, N. Hedin, and L. Bergström, "Structuring adsorbents and catalysts by processing of porous powders," *J. Eur. Ceram. Soc.*, vol. 34, no. 7, pp. 1643–1666, 2014.

[67] B. Valizadeh, T. N. Nguyen, and K. C. Stylianou, "Shape engineering of metal–organic frameworks," *Polyhedron*, vol. 145, pp. 1–15, 2018.

[68] J. Ren, N. M. Musyoka, H. W. Langmi, A. Swartbooi, B. C. North, and M. Mathe, "A more efficient way to shape metal-organic framework (MOF) powder materials for hydrogen storage applications," *Int. J. Hydrogen Energy*, vol. 40, no. 13, pp. 4617–4622, 2015.

[69] C. Perego and P. Villa, "Catalyst preparation methods," *Catal. Today*, vol. 34, no. 3–4, pp. 281–305, 1997.

[70] J. P. DeLuca and L. E. Campbell, "Monolithic Catalyst Supports," in *Advanced Materials in Catalysis*, J. J. Burton and R. L. Garten, Eds. New York: Academic Press, INC, 1977, pp. 293–324.

[71] C. A. Grande, V. I. Águeda, A. Spjelkavik, and R. Blom, "An efficient recipe for formulation of metal-organic Frameworks," *Chem. Eng. Sci.*, vol. 124, pp. 154–158, 2015.

[72] K. Shams and S. J. Mirmohammadi, "Preparation of 5A zeolite monolith granular extrudates using kaolin : Investigation of the effect of binder on sieving / adsorption properties using a mixture of linear and branched paraffin hydrocarbons," vol. 106, pp. 268–277, 2007.

[73] M. W. Kasture, P. S. Niphadkar, V. V Bokade, and P. N. Joshi, "On the catalytic performance in isopropylation of benzene over H / b zeolite catalysts : Influence of binder," vol. 8, pp. 1003–1008, 2007.

[74] A. Aranzabal, D. Iturbe, M. Romero-Sáez, M. P. González-Marcos, J. R. González-Velasco, and J. A. González-Marcos, "Optimization of Process Parameters on the Extrusion of Honeycomb Shaped Monolith of H-ZSM-5 Zeolite," *Chem. Eng. J.*, vol. 162, no. 1, pp. 415–423, 2010.

[75] Y. Y. Li, S. P. Perera, B. D. Crittenden, and J. Bridgwater, "The effect of the

binder on the manufacture of a 5A zeolite monolith," vol. 116, pp. 85–96, 2001.

[76] D. P. Serrano, R. Sanz, P. Pizarro, I. Moreno, P. de Frutos, and S. Blázquez, "Preparation of extruded catalysts based on TS-1 zeolite for their application in propylene epoxidation," vol. 143, pp. 151–157, 2009.

[77] G. Rioland, P. Dutournié, D. Faye, T. J. Daou, and J. Patarin, "Prediction of the mechanical properties of zeolite pellets for aerospace molecular decontamination applications," *Beilstein J. Nanotechnol.*, vol. 7, pp. 1761–1771, 2016.

[78] J. Goldstein *et al.*, *Scanning Electron Microscopy and X-ray Microanalysis*, 3rd ed., vol. 44, no. 0. Kluwer Academic/Plenum Publishers, 2003.

[79] G. Rioland, T. J. Daou, D. Faye, and J. Patarin, "A new generation of MFI-type zeolite pellets with very high mechanical performance for space decontamination," *Microporous Mesoporous Mater.*, vol. 221, pp. 167–174, 2016.

[80] J. J. Purewal *et al.*, "Increased volumetric hydrogen uptake of MOF-5 by powder densification," *Int. J. Hydrogen Energy*, vol. 37, no. 3, pp. 2723–2727, 2012.

[81] C. A. Grande, G. Mondino, A. Lind, Ø. Vistad, and D. Akporiaye, "Selective Removal of CH4 from CH4/CO/H2 Mixtures," in *Small-Scale Gas to Liquid Fuel Synthesis*, no. 1, 2015, pp. 1–48.

[82] L. Ohlin, P. Bazin, F. Thibault-Starzyk, J. Hedlund, and M. Grahn, "Adsorption of CO2 , CH4 , and H2O in Zeolite ZSM-5 Studied Using In Situ ATR-FTIR Spectroscopy," *J. Phys. Chem. C*, vol. 117, no. 33, pp. 16972–16982, 2013.

[83] D. H. Olson, W. O. Haag, and W. S. Borghard, "Use of water as a probe of zeolitic properties: Interaction of water with HZSM-5," *Microporous Mesoporous Mater.*, vol. 35–36, pp. 435–446, 2000.

[84] V. Bolis, C. Busco, and P. Ugliengo, "Thermodynamic study of water adsorption in high-silica zeolites.," *J. Phys. Chem. B*, vol. 110, no. 30, pp. 14849–59, 2006.